UNIVERSITE DE NANTES **FACULTE DES SCIENCES**

M1 BE Bioproduction des écosystèmes

GENETIQUE ET DYNAMIQUE DES POPULATIONS

Illustrations cours Dynamique

Prof. P. G. Beninger

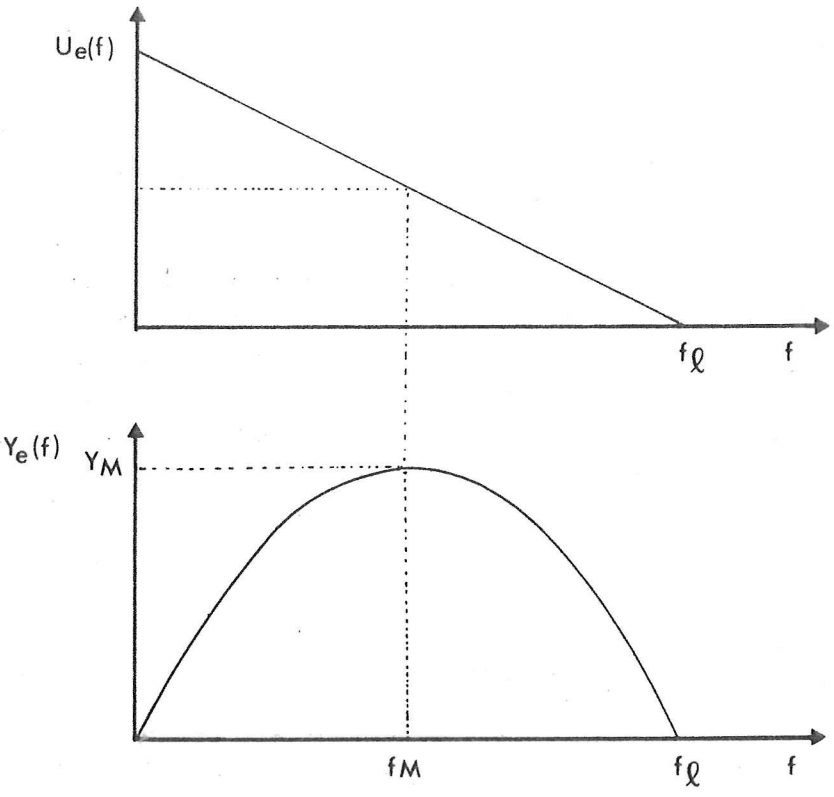

Types de Croissance Démographique

(1) Type r

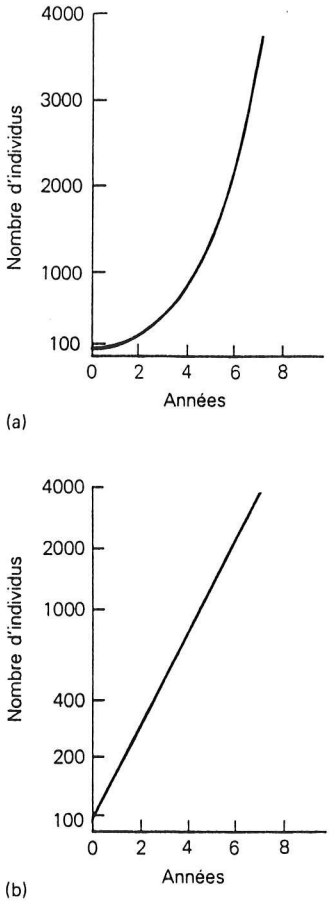

Figure 29-3 Croissance exponentielle d'une population hypothétique, exprimée selon (a) une échelle linéaire et (b) une échelle logarithmique. Dans une croissance exponentielle, la population augmente à un taux toujours croissant. L'équation décrivant ces graphiques est la suivante:

$$* \quad \frac{dN}{dt} = rN$$

où $\frac{dN}{dt}$ = augmentation de la taille de la population par unité de temps
r = taux intrinsèque d'accroissement naturel
N = taille de la population

* Après intégration,

$$N_t = N_0 e^{rt}$$

(2) Type K

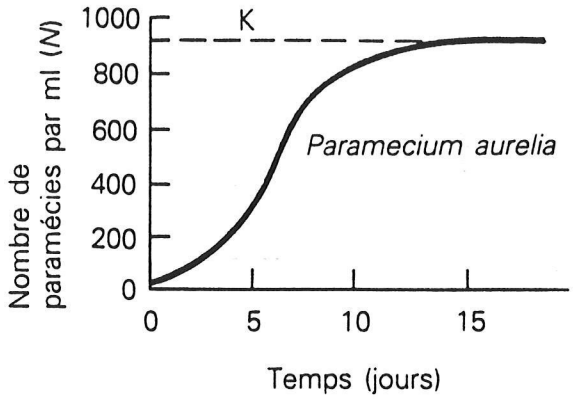

$$* \quad \frac{dN}{dt} = rN\left(\frac{K - N}{K}\right)$$

où: N = nombre d'individus (ou densité de population)

$\frac{dN}{dt}$ = variation du nombre d'individus ou de la densité par unité de temps (c'est-à-dire le taux de croissance de la population)

r = taux intrinsèque d'accroissement naturel

K = capacité limite

L'expression $\frac{(K - N)}{K}$ (résistance de l'environnement) indique la quantité de ressources qui est encore disponible pour la population. Quand N est beaucoup moins élevé que K, l'expression $\frac{(K - N)}{K}$ tend vers 1 et l'équation devient $\frac{dN}{dt} = rN$ (l'équation décrivant la croissance exponentielle). À mesure que N tend vers K, l'expression $\frac{(K - N)}{K}$ tend vers zéro, et $\frac{dN}{dt}$ (c'est-à-dire le taux de croissance) devient nul.

* Après intégration,

$$N_t = \frac{K}{1 + e^{a - rt}}$$

(a = constante d'intégration)

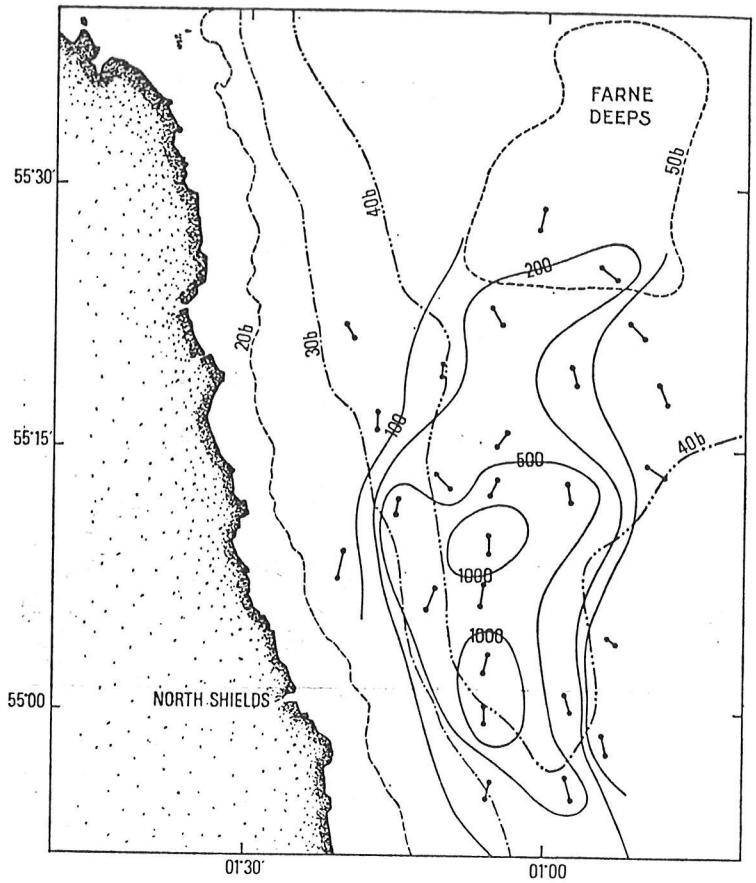

FIG. 1-15. — *Langoustines* (Nephrops norvegicus) : *distribution sur les fonds de pêche de North Shields en mer du Nord d'après les chalutages du N.O. Tellina, en Octobre 1969.* Les emplacements des traits de chalut sont indiqués. Isoplèthes en nombre d'individus pour une demi-heure de pêche. Isobathes en brasses (1,83 m). D'après SYMONDS, 1972.

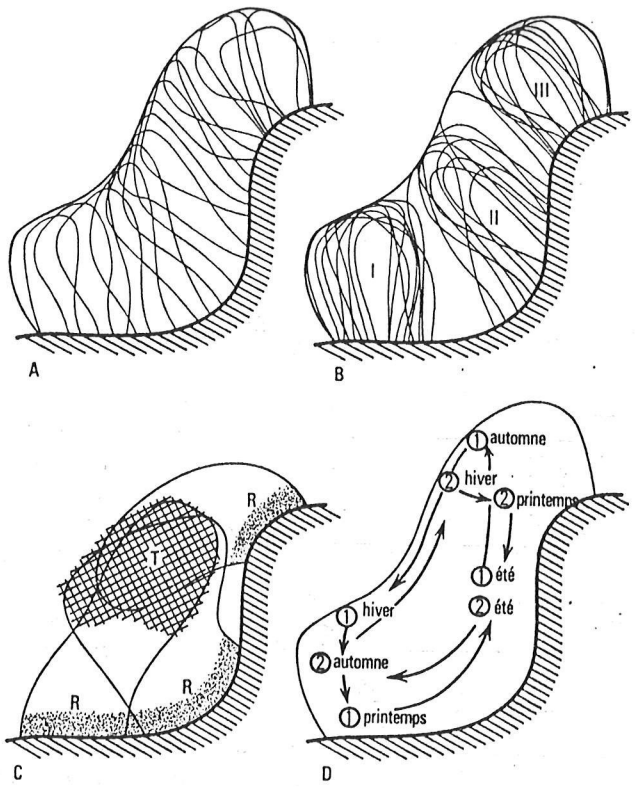

FIG. 1-19. — *Aires géographiques:* A : aire spécifique formant l'enveloppe des aires individuelles; B : aires individuelles mettant en évidence 3 stocks différents (I, II, III); C : aires de 3 stocks différents possédant des aires reproductrices (R) différentes mais une aire trophique commune (T); D : deux stocks 1 et 2 différents occupant l'aire géographique commune en des saisons différentes.

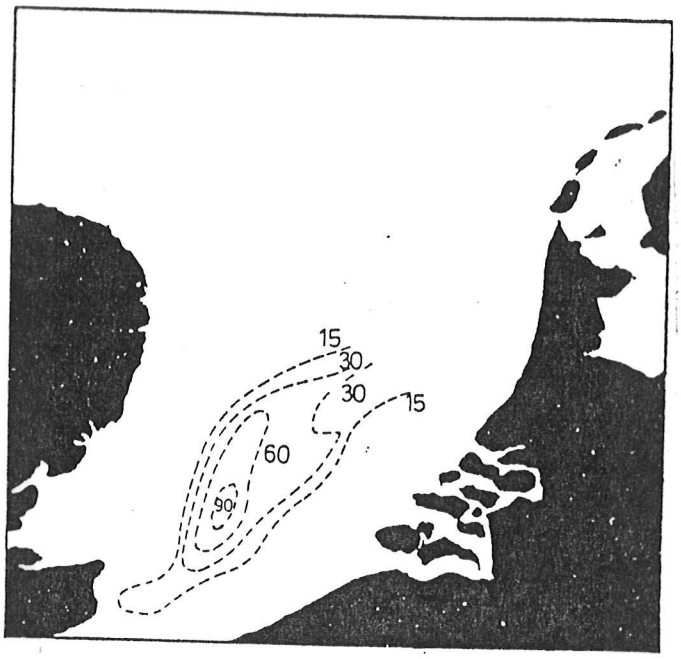

Figure 8.32. Egg density contours for plaice in southern North Sea. Numerals give number of eggs per m^3 *of water.*

(From Wollaston, H. J. B.[42] by permission of the Controller H.M. Stationer Office)

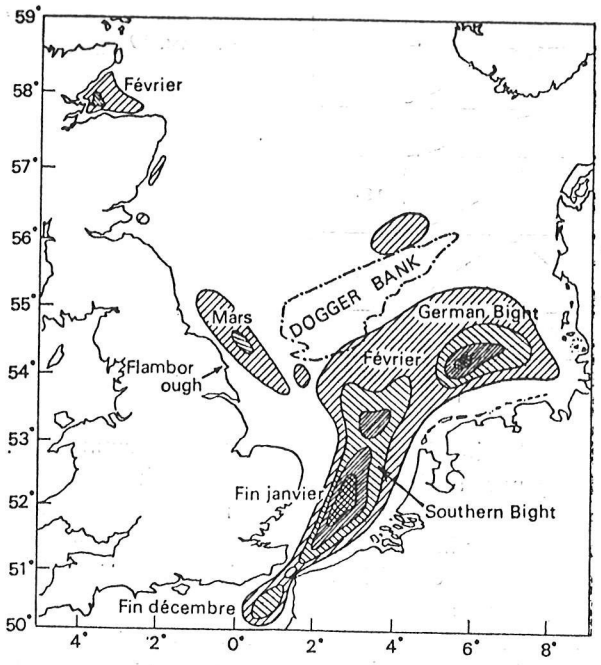

FIG. 1-74. — *Plie* (Pleuronectes platessa) : *aires de ponte en mer du Nord.* Les isoplèthes correspondent à des densités croissantes d'œufs. L'isobathe du Dogger Bank correspond à 20 brasses (environ 37 m). D'après les données de SIMPSON, *in* CUSHING, 1968.

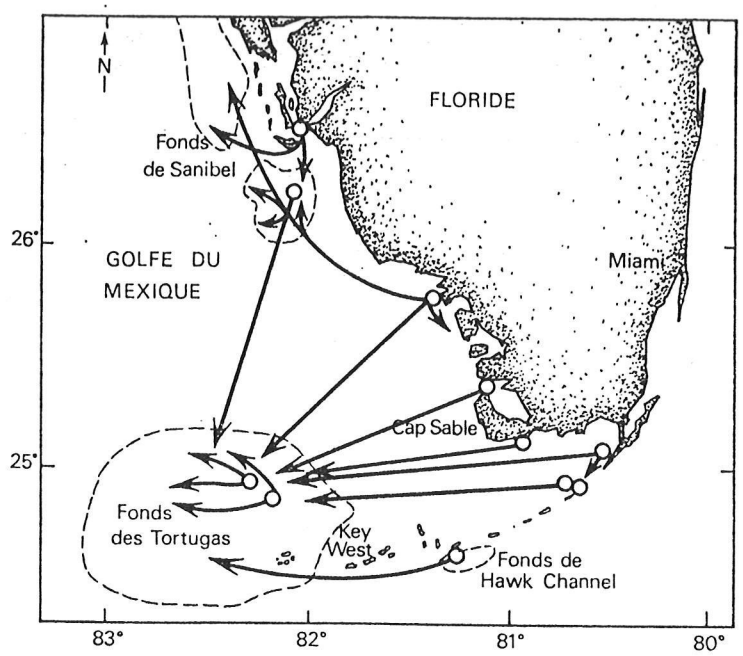

FIG. 1-10. — *Crevettes: migration de* Penaeus duorarum *dans les eaux de la Floride. Les crevettes juvéniles effectuent des migrations allant jusqu'à 150 milles marins pour atteindre les fonds où elles sont pêchées.* Cercles : points de lâcher; flèches : routes migratoires supposées, les pointes correspondant aux lieux de recaptures. Sur la côte est de la Floride toutes les crevettes marquées furent retrouvées à proximité immédiate des points de lâchers. D'après COSTELLO et ALLEN in TEMPLE, 1973.

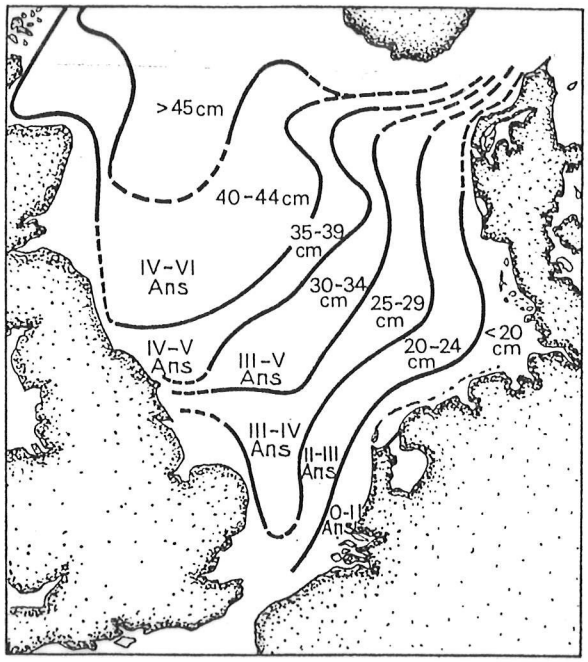

FIG. 1-76. — *Plie* (Pleuronectes platessa) : *carte donnant l'âge moyen et la taille moyenne pour les différentes zones de la mer du Nord.* Les jeunes poissons sont cantonnés dans les nourriceries côtières. D'après GARSTANG, *in* HARDY, 1959.

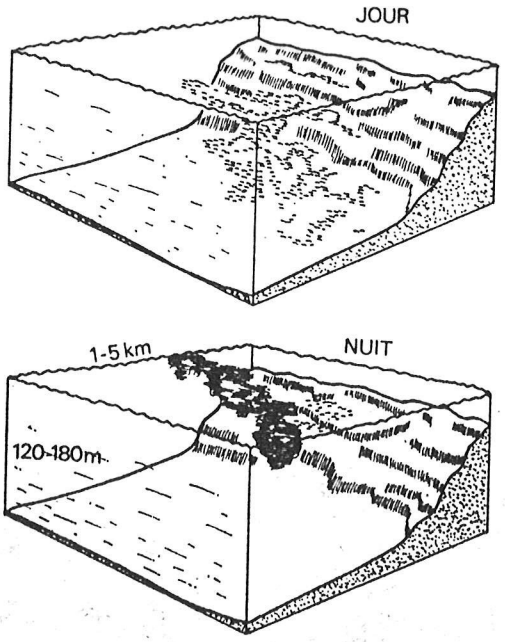

FIG. 1-24. — *Hareng de l'Atlantique* (Clupea harengus harengus) : *interprétation de la répartition spatiale d'un « groupe » de hareng pendant le jour et pendant la nuit à partir d'enregistrements effectués au Sonar à longue distance* (GLORIA) *et d'échosondages.* La zone représentée se situe au large du banc Hawes, dont la pente nord est figurée (à l'ouest de l'Écosse, au sud des Hébrides) et correspond à une surface variant entre 1 et 25 km², suivant la taille et la densité du « groupe » de hareng choisi. Réparti de jour en petits bancs dispersés et profonds le « groupe » se concentre de nuit en grands bancs superficiels présentant des masses pendulaires descendant plus profondément. D'après ROSBY *et al.*, 1973.

La distribution spatiale

- La matière et l'énergie de l'univers ne sont distribuées ni de façon aléatoire, ni de façon régulière, à aucune échelle ; la distribution groupée est la norme
- *Idem* pour les organismes terrestres et marins, seules qqs exceptions à qqs échelles (ex. territorialité)
- La distribution spatiale d'un caractère donné se situe quelque part sur le spectre *contiguité-fragmentation*
- L'analyse de la distribution spatiale fait partie de la *statistique spatiale*, branche de la statistique très différente de la statistique experimentale conventionnelle
- Les techniques de la statistique spatiale évoluent très rapidement
- Technique à **proscrire** : rapport moyenne-variance
- Technique dépassée : NND (nearest neighbour distance)
- Techniques conseillées : Autocorrélation (ex. Moran's *I*), semivariance - analyse fractale, krijage
- Ces techniques peuvent caractériser différents paramètres des distributions spatiales : taille des patchs, distance inter-patch, degré de réplication de la distribution groupée à des échelles différentes
- Les activités anthropiques peuvent impacter les distributions spatiales ; ces altérations peuvent être des signes précurseurs de dysfonctionnements écosystémiques conséquents

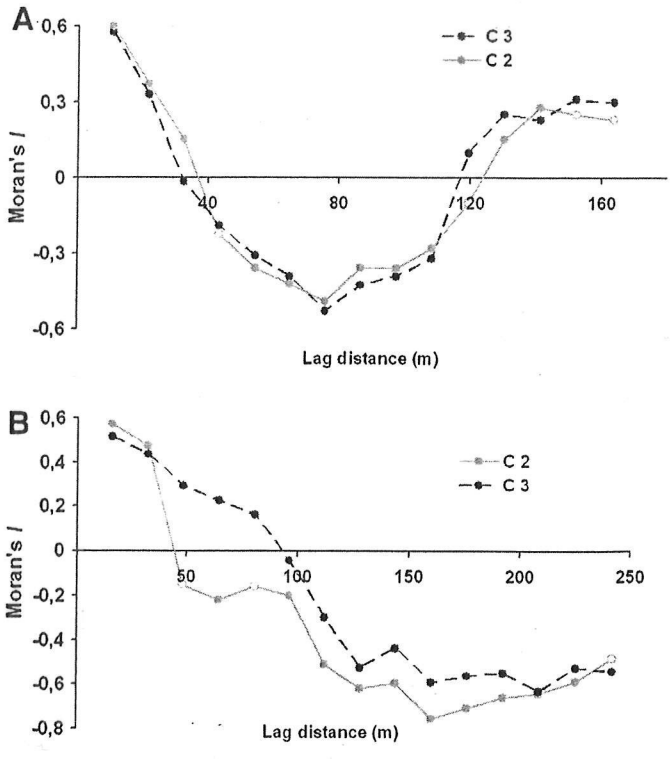

Fig 2. Spatial autocorrelograms for *T. philippinarum* densities. A. Reference site. B. Impacted site. C2 is presented by solid line, C3 by dashed line. Significant values are represented by solid circles, non-significant values are represented by empty circles.

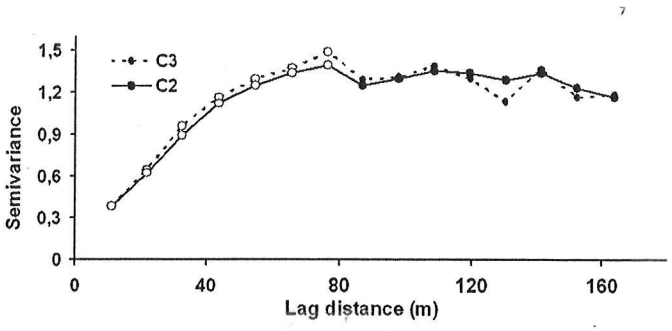

Fig 3. *Tapes philippinarum*, reference site. Experimental variograms for C2 and C3 cohorts. Open circles show the points used for calculating the fractal dimension.

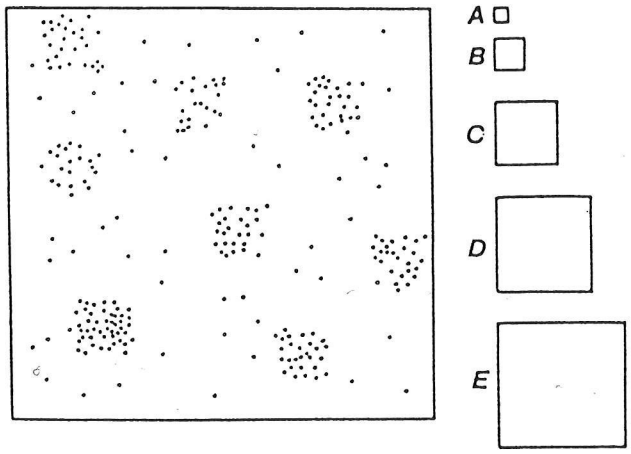

Fig. 7.3. The relationship between quadrat size and ~~variance~~ (see text).

distribution analysis

Méthodes d'estimation des nombres

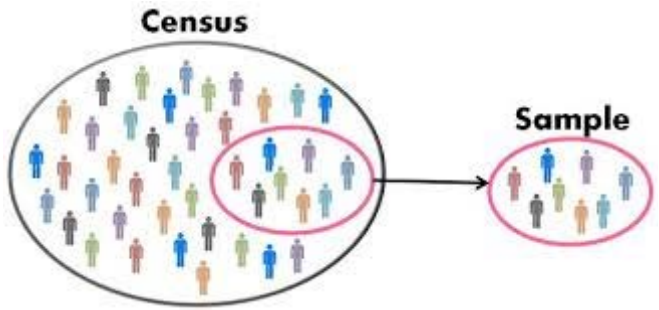

Recensement

Echantillon,
indirect

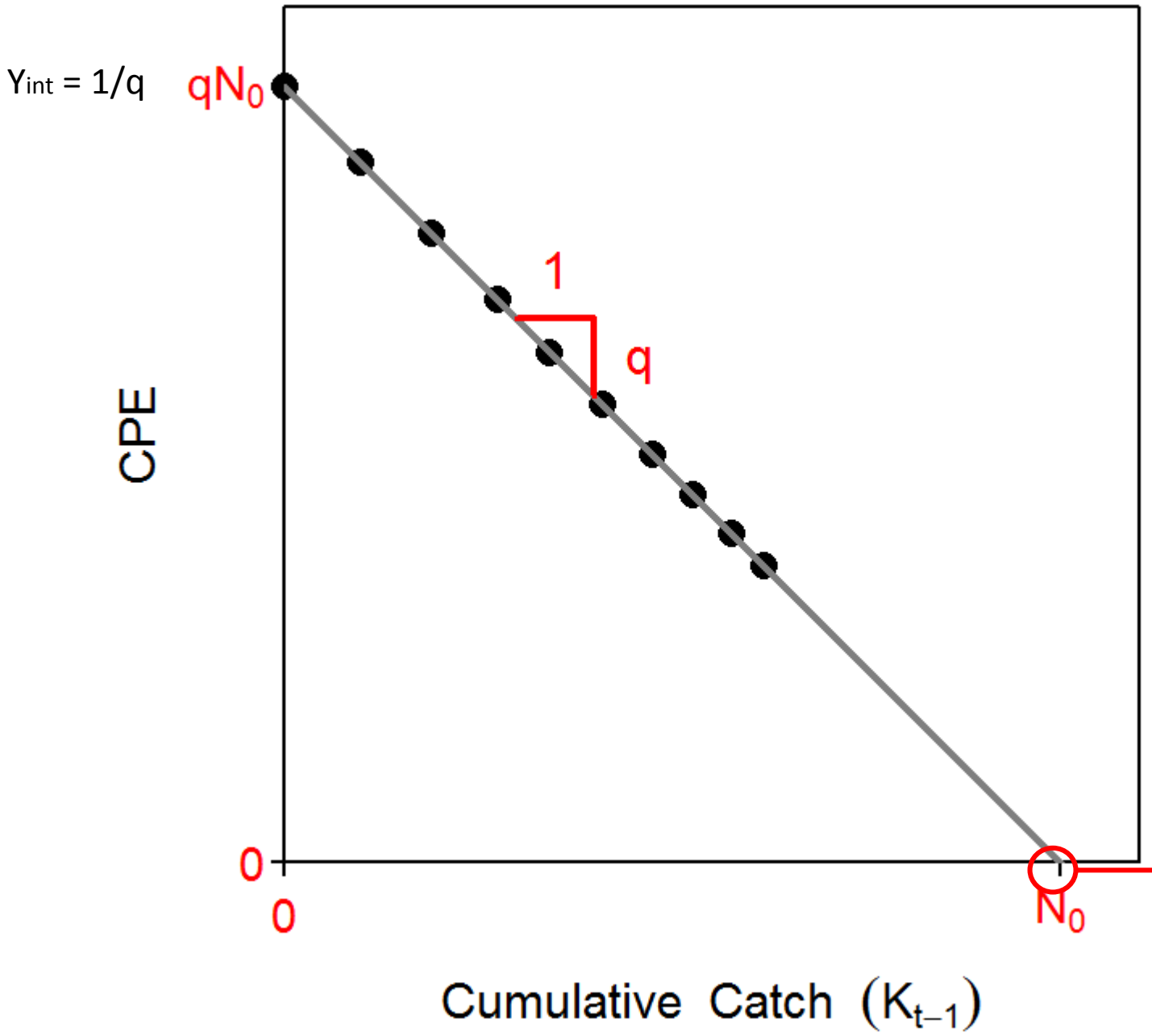

Projection, comme si on avait réussi à capturer tous les animaux, avec 0 mortalité naturelle pendant l'intervalle de temps de l'étude

Estimating Animal Numbers

Removal Methods

- Leslie Method

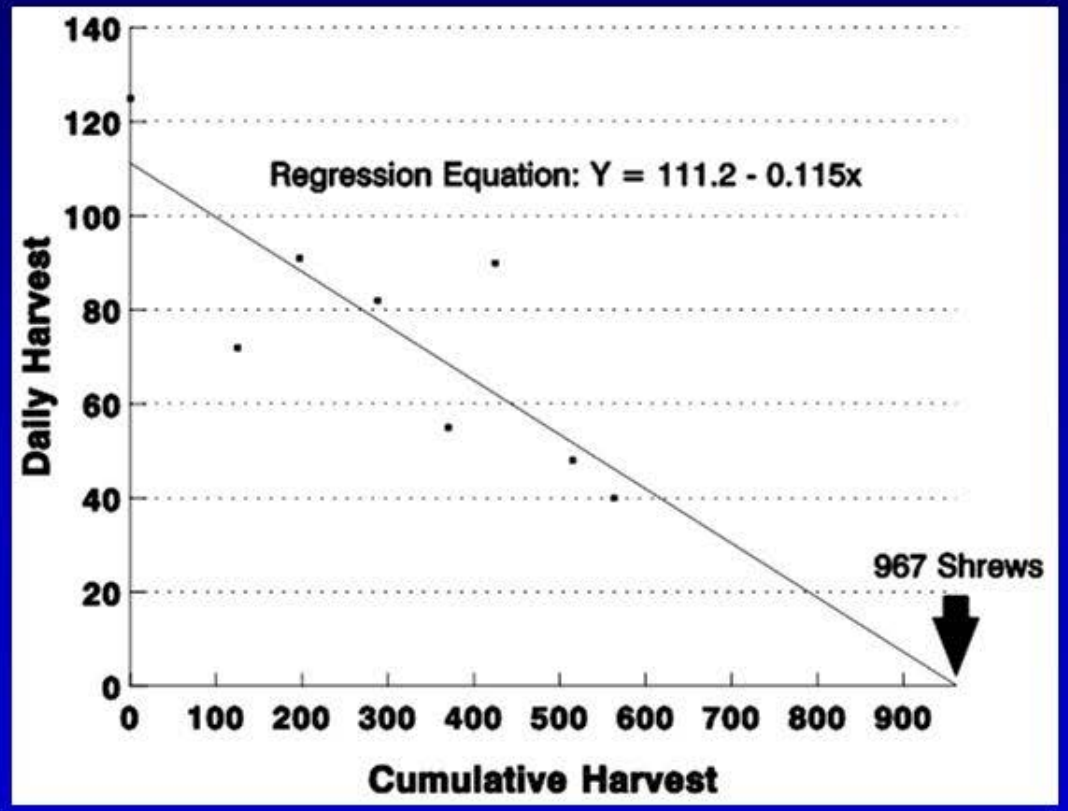

CPUE vs. $C_{cumulé}$

q = 0.115
Y-int = 111.2

ε: structure, autocorrelation, linéarité en variables et en forme…

Estimation des nombres: capture-recapture

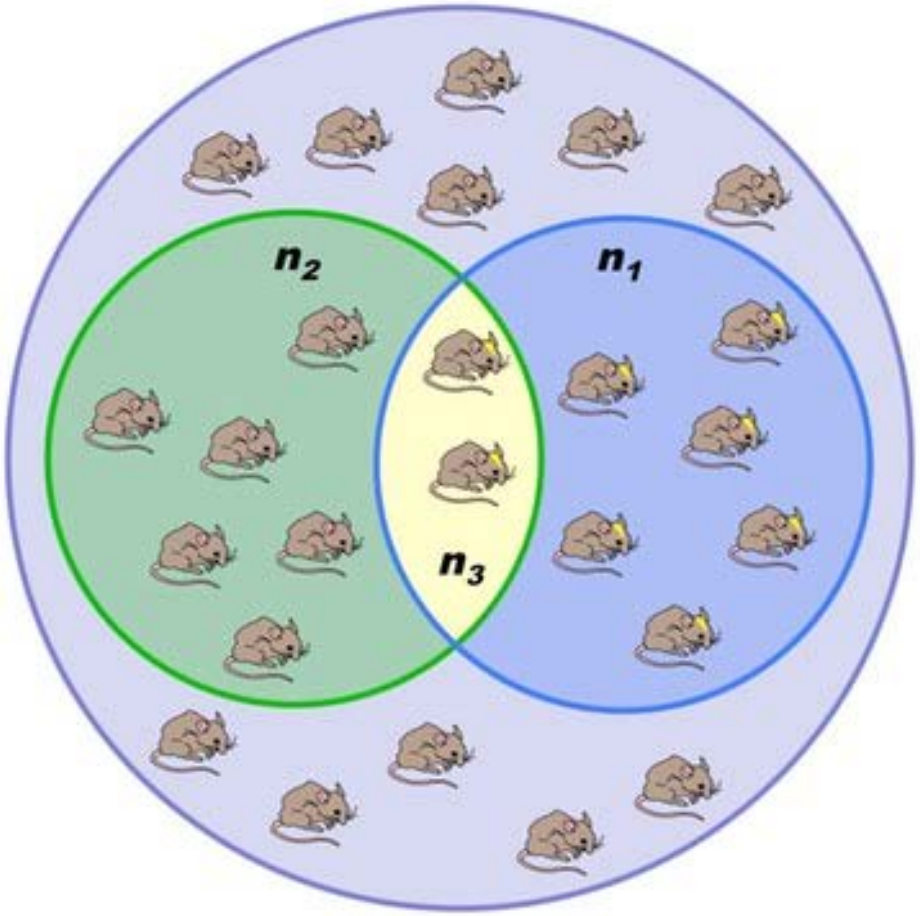

Total Population

First Capture (n_1)

Second Capture (n_2)

Recaptures (n_3)

$$N_{pop} = \frac{N_{capt} \times N_{marqué}}{N_{capt\ avec\ marque}}$$

Table 10.1 Catch and effort during a depletion experiment at Woleai Atoll, Federated States of Micronesia where surgeonfishes (Acanthuridae) were depleted by spearfishing (Smith & Dalzell, 1993).

Day	Effort (person h)	Catch (kg)	CPUE (kg h^{-1})	Cumulative catch (kg)
1	30.75	18.44	0.60	18.44
2	23.92	12.73	0.53	31.17
3	24.50	8.61	0.35	39.78
4	25.08	8.04	0.32	47.82

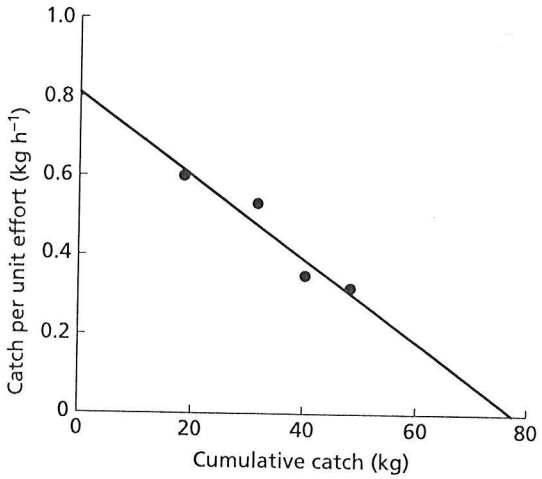

Fig. 10.10 Depletion plot for surgeonfishes caught by spear fishing at Woleai Atoll. Data from Smith and Dalzell (1993).

Les nombres dans une série temporelle

- Des mesures ponctuelles ne peuvent donner de renseignements précis (c.a.d. statistiquement acceptables) sur les variations dans le nombre d'individus d'un ensemble au cours du temps
- Pourtant, ceci est très souvent , très exactement, ce que nous recherchons comme donnée de base pour la compréhension de la dynamique d'un ensemble
- Il est donc nécessaire de faire des estimations de N répétées au cours du temps (ex tous les mois, tous les ans).
- Nous avons tendance à penser qu'il suffit de faire un ANOVA suivi d'une comparaison multiple pour pouvoir déceler des différences significatives dans le N à des moments temporellement séparés ; beaucoup d'auteurs l'ont fait
- Or, ces données sont toujours autocorrelées à des degrés inconnus ; il est donc **impossible** de faire de telles analyses statistiques
- Il n'existe aucune technique statistique permettant de le faire
- Dans le cas de phénomènes cycliques, il est possible de caractériser les cycles (ex : analyse en wavelets), mais toujours pas de comparer directement les nombres d'individus

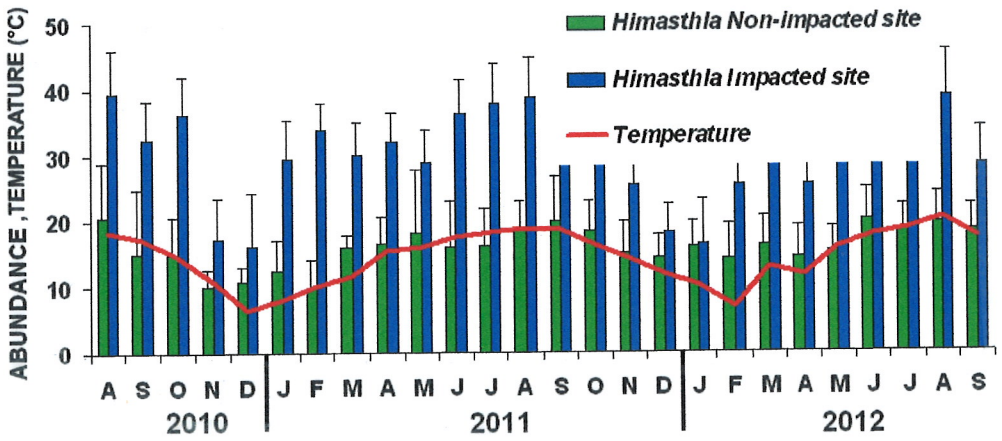

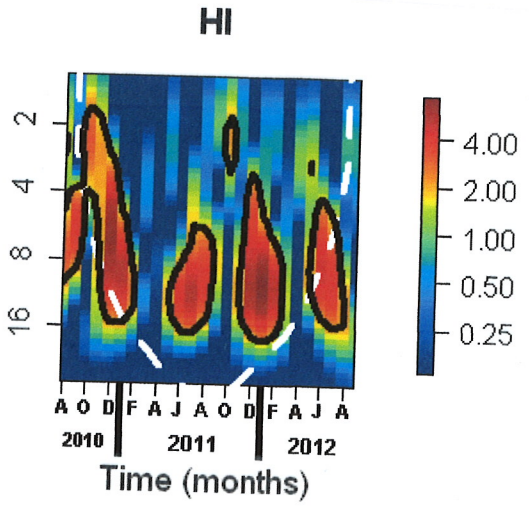

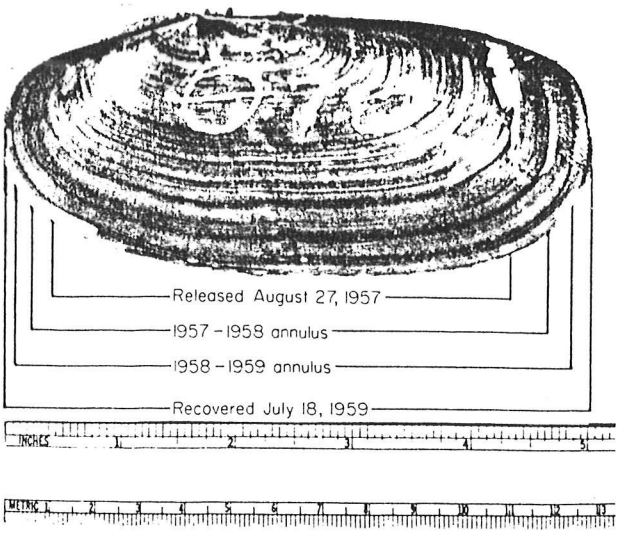

Fig. 4.25. A numbered razor clam, *Siliqua patula*, added two clear annuli to its shell before recapture. (Photo by Herb C. Tegelberg, Washington Dept. of Fisheries, Olympia, Washington.)

Fig. 4.23. A scale of a mature sockeye salmon, *Oncorhynchus nerka*, from Bristol Bay, Alaska. Shown are the focus (F) of the scale, one annulus near the end of freshwater life (1) and three annuli during saltwater life (2, 3, 4). (Photo by Ted S. Y. Koo, Fisheries Research Institute, University of Washington, Seattle, Washington.)

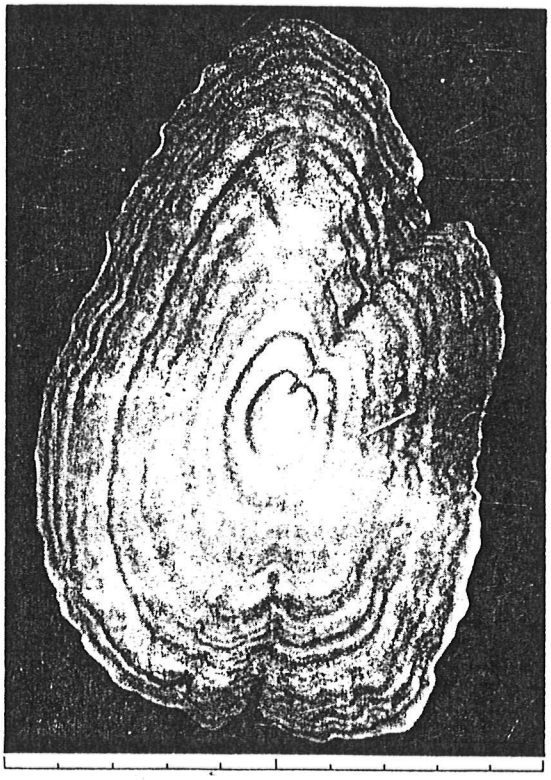

Fig. 4.24. An otolith of a 12-year-old Pacific halibut, *Hippoglossus stenolepis*. (Photo by International Pacific Halibut Commission, Seattle, Washington.)

Marine Biology 107, 439–442 (1990)

Potential of morphological lipofuscin age-pigment as an index of crustacean age

M. R. J. Sheehy

Zoology Department, University of Queensland, St. Lucia, Brisbane 4067, Australia

Date of final manuscript acceptance: June 15, 1990. Communicated by G. F. Humphrey, Sydney

Abstract. Morphological lipofuscin concentration in the brains of laboratory-reared crayfish, *Cherax quadricarinatus* (von Martens), of known age, was quantified using alternative fluorescence microscope and image-analysis techniques. The quantity of olfactory-lobe lipofuscin was highly correlated with age ($r = 0.96$). It was found to be a superior predictor of age compared with the body-size parameters frequently used for this purpose. The results of this study suggest that morphological lipofuscin, quantified by image analysis, has significant potential as a means of age determination for crustaceans.

Marine Biology (1994) 121: 237–245

M. R. J. Sheehy · J. G. Greenwood · D. R. Fielder

More accurate chronological age determination of crustaceans from field situations using the physiological age marker, lipofuscin

Received: 27 June 1994 / Accepted: 21 July 1994

Abstract A captive population of Australian red-claw crayfish, *Cherax quadricarinatus*, of known age was used for the study. Lipofuscin concentration in the left olfactory lobe cell mass of the brain was measured using image analysis of fluorescence micrographs. Age predictions based on lipofuscin concentration were more accurate and had narrower 95% confidence limits than those derived from the more conventional body size and weight predictors for all age groups tested (180, 300, 420, 780 d). Overall, use of lipofuscin concentration produced a significantly lower ($p < 0.001$) mean age-prediction error (16.65%) than use of carapace length or body weight (32.45 and 32.3%, respectively). Carapace length was of little value for prediction of the age of older individuals. Mathematical models defining the relationships between temperature, age and lipofuscin accumulation were derived from laboratory-reared individuals. These models did not describe adequately the course of lipofuscin accumulation in crayfish from the field over the whole lifespan. Field data from three "known" year-classes were used to generate simulated size-frequency and lipofuscin concentration-frequency histograms. Year-classes in the lipofuscin concentration frequency-histogram were much more easily distinguished than in the size-frequency histogram. Under field conditions, lipofuscin concentration was a better predictor of chronological age than conventional morphometric measures.

Table 1 *Cherax quadricarinatus.* Optimal parameter values for seasonalized von Bertalanffy models and adjusted coefficients of variation for field data. (Y_∞ asymptotic value of predictor variable; C amplitude of seasonal oscillation; K curvature factor; t_0 theoretical age at which predictor variable=0; t_s summer point or fraction of year which has passed before rate of increment in predictor variable is maximal; V adjusted coefficient of variation with subscript indicating age group)

Predictor variable	Seasonalized von Bertalanffy parameter					Adjusted coefficient of variation			
	Y_∞	C	K	t_0	t_s	V_{180d}	V_{300d}	V_{420d}	V_{780d}
Lipofuscin concentration	25.91	0.812	0.084	0.169	0.859	61.7	22.1	18.2	22.2
Carapace length	59.79	0.771	1.221	0.025	0.949	89.8	38.2	14.5	10.7
Body weight	124.7	1	0.179	0.160	0.960	108.2	67	36	23.7

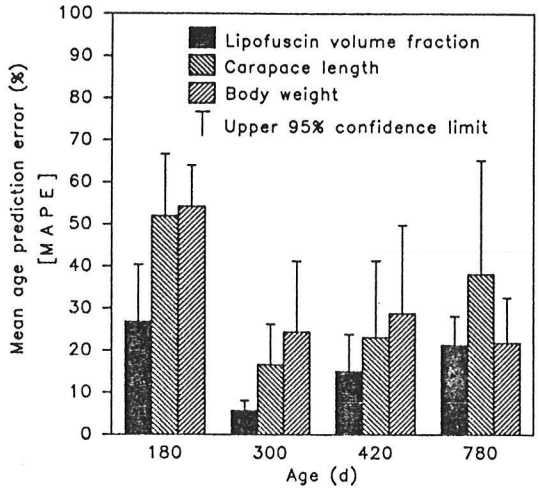

Fig. 2 *Cherax quadricarinatus.* Mean age prediction errors (MAPE) for experimental field crayfish of four age groups (180, 300, 420 and 780 d) after back-calculation from optimally fitted seasonalized von Bertalanffy models

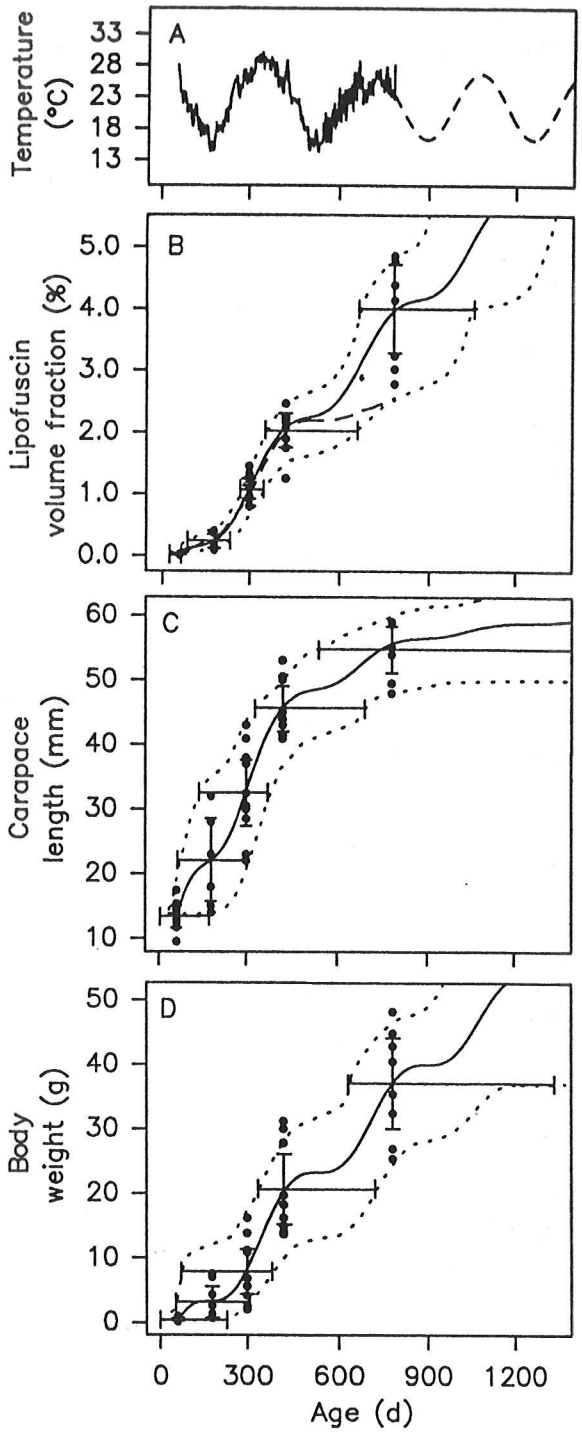

Fig. 1 *Cherax quadricarinatus.* Mean daily water temperatures at field site (**A**) and relationship between age and olfactory lobe cell-mass lipofuscin concentration (**B**), carapace length (**C**), and body weight (**D**) in experimental field population. Also shown are vertical 95% confidence limits for mean of each age group. Data are optimally fitted with seasonalized von Bertalanffy models (continous lines). Dashed portion of line in **A** represents predicted future average water temperatures, and in **B** predicted lipofuscin accumulation based on thermal-age models derived from laboratory data (*Dotted lines enclosing horizontal bars* 95% confidence limits for inverse prediction of ages from dependent variables; *confidence bands above oldest samples* putative only)

Vol. 428: 161–176, 2011
doi: 10.3354/meps09055

MARINE ECOLOGY PROGRESS SERIES
Mar Ecol Prog Ser

Published May 3

Use of extractable lipofuscin to estimate age structure of ghost shrimp populations in west coast estuaries of the USA

Katelyn M. Bosley[1,*], Brett R. Dumbauld[2]

[1]Oregon State University, Hatfield Marine Science Center, 2111 S.E. Marine Science Drive, Newport, Oregon 97365, USA
[2]US Department of Agriculture, Agricultural Research Service, 2030 S.E. Marine Science Drive, Newport, Oregon 97365, USA

ABSTRACT: Determining age in crustaceans is inherently imprecise because they molt periodically and do not retain hard structures throughout their lifespan. Morphological measurements are often used to estimate age, but variability in individual growth rate and molt frequency can result in a wide distribution of sizes in a single age class, making size a poor predictor of true age. Concentration of the autofluorescent age pigment, lipofuscin, has been shown to be directly related to actual age in many crustaceans. The present study assessed the potential of using extractable lipofuscin as a method for determining age in the ghost shrimp *Neotrypaea californiensis*. Following validation of the technique, lipofuscin-based aging was used to determine age structures for 3 populations of *N. californiensis*, and these were compared to age structures determined using traditional length-based methods. Analysis of lipofuscin revealed up to 13 age classes where the size-based analysis showed only 7. Comparison of mean size-at-age among populations in Oregon and Washington estuaries demonstrated that growth rate varied spatially, probably responding to site-specific environmental factors like food availability and population density. *N. californiensis* negatively impact oyster aquaculture in Pacific Northwest estuaries. Analysis of extractable lipofuscin proved to be a more accurate method of age determination than body-length measurements and should facilitate more in-depth investigations of basic biological and ecological processes, which will benefit current efforts to develop an integrated pest management plan for *N. californiensis*.

$$\text{Age (yr)} = \frac{[\text{LF index (ng } \mu\text{g}^{-1}) + 0.064]}{0.21}$$

Gompertz: $$L_t = L_\infty \cdot e^{-e^{[-K\bullet(t-t_0)]}} \quad (1)$$

Special VBGF: $$L_t = L_\infty \cdot \left(1 - e^{-K\cdot(t-t_0)}\right) \quad (2)$$

Richards: $$L_t = L_\infty \cdot \left[1 - D \cdot e^{[-K\cdot(t-t_i)]}\right]^{\frac{1}{D}} \quad (3)$$

Logistic: $$L_t = \frac{L_\infty}{\left(1 + e^{-K\cdot(t-t_0)}\right)} \quad (4)$$

Generalized VBGF: $$L_t = L_\infty \cdot \left(1 - e^{-K\cdot(t-t_0)}\right)^D \quad (5)$$

L_∞ : asymptotic length [mm],
K, $D_{Richards}$: growth parameters [yr^{-1}],
$D_{Gen.VBGF}$: surface factor,

t : age [yrs],
t_0 : theoretical age at zero length,
t_i : age at the inflexion point [yr]

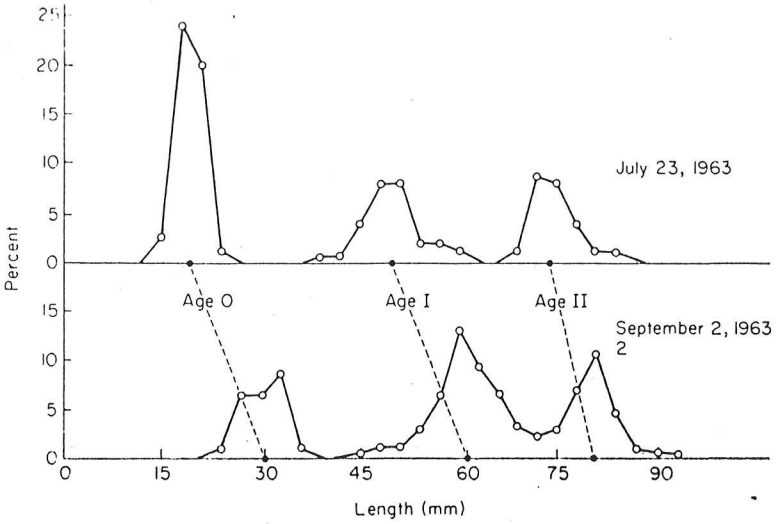

Fig. 4.22. Percentage length frequencies of pond smelt, from Black Lake, Alaska, in mid and late summer. (Unpublished data from Fisheries Research Institute, University of Washington, Seattle, Washington, 1900).

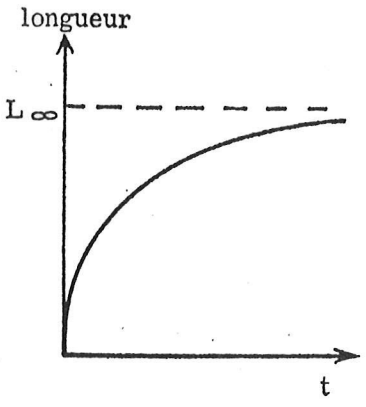

FIGURE 3.1.1. – Courbe de croissance en longueur.

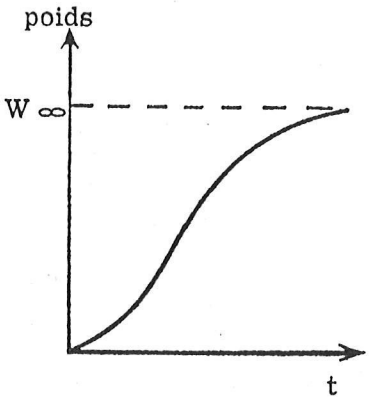

FIGURE 3.1.2. – Courbe de croissance en poids.

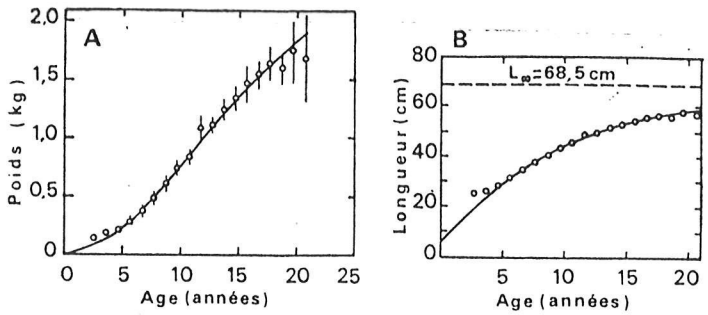

FIG. 1-73. — *Plie* (Pleuronectes platessa) : A, *croissance en poids;* la courbe correspond à l'équation de Von Bertalanffy (cf. § 2-4) avec W_∞ = 2 867 g, k = 0,095 et t_0 = — 0,815 années (la longueur de chaque ligne verticale est égale à 6 fois l'erreur standard de la moyenne et donne donc pour celle-ci un intervalle de confiance avec un coefficient de sécurité supérieur à 99 %). B, *croissance en longueur;* la courbe de Von Bertalanffy correspond à L_∞ = 68,5 cm, k = 0,095 et t_0 = — 0,815 années. N.B. : les échantillons proviennent des marchés de Lowestoft et Grimsby (1929-1938) ce qui explique le biais pour les classes d'âge de 3 et 4 ans, les individus les plus petits étant éliminés. D'après BEVERTON et HOLT, 1957.

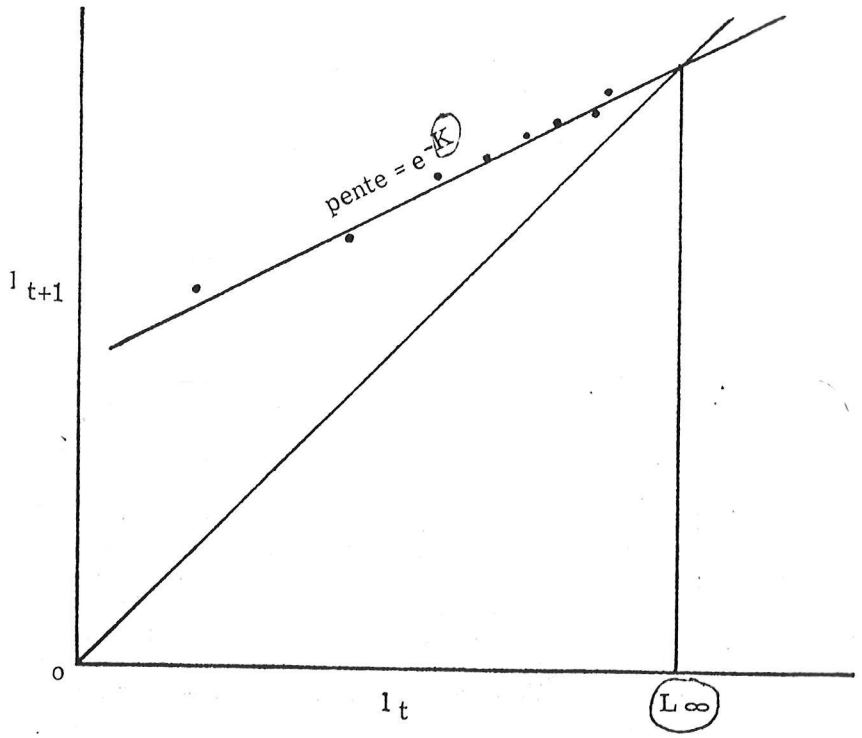

FIGURE 3.2.2. – Estimation des constantes de croissance. Représentation de la longueur par rapport à la longueur un an auparavant (courbe de Ford-Walford).

Table 3. *Placopecten magellanicus.* Summary of parameters for shell height data (mm) presented in Fig. 6 fitted to the Von Bertalanffy equation $H_t = H_\infty[1-e^{-k\,(t-t_0)}]$, where H_t = height at age t; H_∞ = mean asymptotic height; k = Brody growth coefficient; t_0 = a parameter representing time when H_t = zero. Also parameters for somatic weight data (g) fitted to polynomial regression equations, $y = \beta_0 + \beta_1 x + \beta_2 x^2 + \beta_3 x^3$ where x = age of scallop (yr); y = predicted somatic weight (g). Regressions represent pooled yearly samples and are all highly significant ($P \ll 0.001$)

	Sunnyside			Dildo			TNNP			St. Andrews			Colinet	
	10 m (n=272)	20 m (n=256)	31 m (n=243)	10 m (n=121)	20 m (n=148)	31 m (n=137)	10 m (n=114)	20 m (n=122)	31 m (n=94)	10 m (n=83)	31 m (n=73)	76 m (n=58)	6 m (n=280)	16 m (n=207)
Shell height *vs* age (Von Bertalanffy)														
H_∞	176.5	165.5	158.4	175.4	168.2	147.8	163.1	151.1	146.0	166.9	166.0	170.2	158.6	160.1
k	0.19	0.20	0.16	0.19	0.19	0.22	0.24	0.22	0.17	0.21	0.21	0.19	0.18	0.19
t_0	0.55	0.63	0.10	0.66	0.37	0.74	1.26	0.37	−0.88	0.51	0.53	0.20	0.54	0.72
r^2	0.97	0.97	0.97	0.97	0.96	0.97	0.90	0.94	0.92	0.96	0.98	0.97	0.96	0.96
Somatic weight *vs* age (polynomial)														
β_0	21.19	17.96	12.25	27.20	20.25	13.84	19.29	14.48	10.25	9.91	9.45	9.97	12.39	15.13
β_1	2.46	2.08	1.43	2.58	1.84	1.17	1.50	0.92	0.65	2.69	2.70	2.96	1.30	1.60
β_2	−0.14	−0.11	−0.07	−0.18	−0.12	−0.09	−0.13	−0.09	−0.05	−0.04	0.004	0.10	−0.07	−0.12
β_3	−0.005	−0.006	−0.003	–	–	–	–	–	–	–	–	–	–	–
r^2	0.91	0.89	0.87	0.92	0.89	0.88	0.78	0.86	0.72	0.94	0.92	0.95	0.87	0.82

Journal of Shellfish Research, Vol. 19, No. 1, 219–228, 2000.

MICROSTRUCTURE, CHRONOLOGY AND GROWTH OF THE PINTO ABALONE, *HALIOTIS KAMTSCHATKANA*, IN ALASKA

SCORESBY A. SHEPHERD,[1] DOUGLAS WOODBY,[2]
JANET M. RUMBLE,[2] AND MIGUEL AVALOS-BORJA[3]
[1]*South Australian Research and Development Institute, Henley Beach 5022, South Australia*
[2]*Alaska Department of Fish and Game, Douglas, Alaska 99824-0020*
[3]*Centro de Ciencias de la Materia Condensada, Universidad Nacional Autonoma de Mexico, Ensenada 22800, Baja California, Mexico*

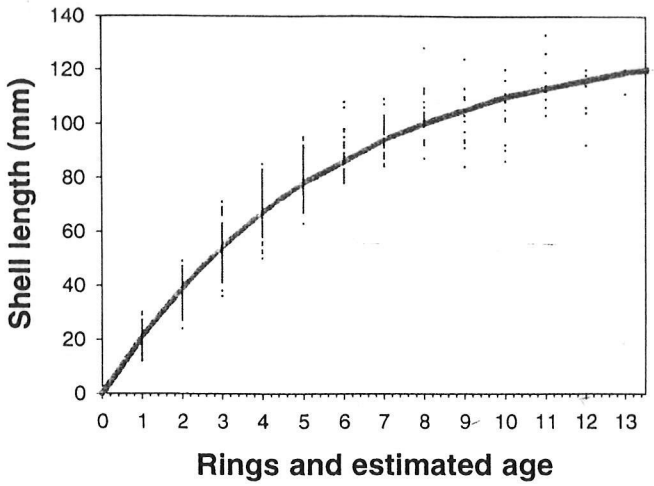

Figure. 9. A plot of a von Bertalanffy growth curve fitted to length-at-age data for all sites combined, and length-increment data from Gravina Island.

TABLE 4.

Parameters of von Bertalanffy growth curves fitted to length-age data for each site.

Site	*N*	K (SE)	L_∞ (SE)
Gravina Island	86	0.21 (0.02)	119.7 (5.6)
Magic Island	103	0.20 (0.01)	129.6 (4.4)
Thimble Cove	110	0.16 (0.01)	136.9 (7.7)
Galankin Island	41	0.22 (0.03)	113.0 (7.7)
Ridge Island	79	0.16 (0.02)	134.9 (13.7)
Battery Island	32	0.25 (0.02)	118.9 (4.2)
Jumbo Island	58	0.19 (0.02)	128.6 (5.5)
Mean value		0.20 (0.01)	125.9 (3.4)
All sites combined	509	0.18 (0.01)	131.9 (2.4)

Journal of Shellfish Research, Vol. 19, No. 1, 57–62, 2000.

MODELING GEODUCK, *PANOPEA ABRUPTA* (CONRAD, 1849) POPULATION DYNAMICS. I. GROWTH

A. HOFFMANN,[1] A. BRADBURY,[2] AND C. L. GOODWIN[3]
[1]*Washington Department of Fish & Wildlife*
600 Capitol Way North
Olympia, Washington 98501
[2]*Washington Department of Fish & Wildlife*
Point Whitney Shellfish Laboratory
1000 Point Whitney Road
Brinnon, Washington 98320
[3]*750 Mountain View Road*
Quilcene, Washington 98376

ABSTRACT In Washington State, target fishing mortality rates (F) for the geoduck clam, *Panopea abrupta* (Conrad, 1849), are based on relative changes in biomass and therefore depend on growth patterns. With these policies, higher growth rates lead to larger harvest quotas so that applying higher rates to areas with slower growth would cause overharvesting. Therefore, in estimating growth patterns, it is important to recognize the scale to which estimates of growth rates should be applied. In this study, we tested whether growth parameters differed among regions and among local sites within regions in Washington, and whether they differed enough to compel managers to create location-specific policies. Von Bertalanffy growth parameters were estimated for 11 sites dispersed among four regions. Among those sites, L_∞ ranged from 13.2 to 17.3 cm, k ranged from 0.113 to 0.235, and t_0 ranged from −0.029 to 0.806. Of the three parameters, the growth constant k had far more influence on target fishing mortality rates (F) than either L_∞ or t_0. Statistically significant differences in k were found among all local sites within geographic regions. However, only some of the differences were of a magnitude to concern management policies. We have proposed a general method for calculating and then testing for managerial significance when a linear relationship exists between k and the fishing mortality rate (F). Our results implied that managerially significant differences in k existed among local sites within Washington's geoduck management regions, posing a dilemma for managers who, by convention, propose a single target fishing mortality rate for each region.

KEY WORDS: Geoduck, growth, hypothesis testing, managerial significance, *Panopea abrupta*, von Bertalanffy

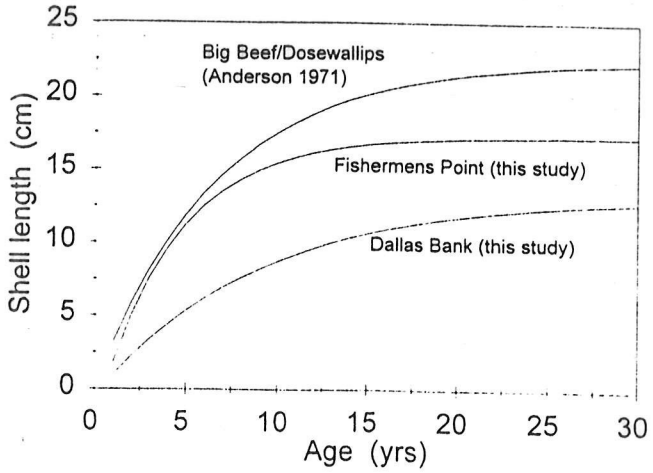

Figure 4. The von Bertalanffy growth curves for geoduck growth at the fastest growth site (Fishermans Point) and the slowest growth site (Dallas Bank) in this study. Also shown is Anderson's (1971) growth curve for Big Beef/Dosewallips.

TABLE 1.

Sample size, mean shell length and von Bertalanffy growth parameter estimates (±SE) derived from shell length at age for *P. abrupta* at 11 sites in Washington.

Region	Site	No. Dug	No. Subsampled	Mean Shell Length (cm)	L_∞ (cm)	k	t_0
South Sound	Hunter Point	71	21	15.2	16.4 (± 0.357)	0.2283 (± 0.009)	0.719 (± 0.040)
	Herron Island	36	23	12.5	13.2 (± 0.158)	0.1544 (± 0.006)	0.422 (± 0.074)
Central Sound	Agate Passage	208	20	13.6	15.8 (± 0.383)	0.1964 (± 0.009)	0.183 (± 0.066)
	Blake Island	19	18	13.0	14.6 (± 0.283)	0.1586 (± 0.006)	0.806 (± 0.071)
Hood Canal	Bangor	98	25	13.5	14.3 (± 0.252)	0.1569 (± 0.007)	0.545 (± 0.055)
	Tala Point	96	24	12.4	13.6 (± 0.361)	0.1435 (± 0.009)	−0.029 (± 0.071)
	Port Gamble (dredged)	180	21	13.1	15.2 (± 0.283)	0.1810 (± 0.007)	0.661 (± 0.052)
	Port Gamble (control)	80	21	12.7	14.0 (± 0.390)	0.1610 (± 0.007)	0.599 (± 0.075)
	Thorndyke Bay	258	21	12.2	13.0 (± 0.201)	0.1421 (± 0.005)	0.550 (± 0.097)
	Fishermans Point	21	19	16.8	17.3 (± 0.251)	0.2353 (± 0.009)	0.552 (± 0.059)
Strait	Dallas Bank	149	21	12.0	13.3 (± 0.405)	0.1131 (± 0.005)	0.334 (± 0.096)

Allométrie: vitesses de croissance ≠

Ex: largeur carapace (LC) vs largeur pince (LP) (Décapodes)
poids frais (W) vs longueur (L) (Poissons)

Modelisation:

Equation allométrique poids : taille 'Big Mac': $W = aL^b$ 'Power Law'

ou

$\text{Log } W = \text{Log } a + b \text{ Log } L$

Problèmes:

1. Il peut y avoir d'autres modèles plus performantes (*voir Katsanevakis 2007*)
2. Les régressions linéaires sont souvent effectuées sans égards pour les suppositions, l'opportunité de transformation log, l'autocorrélation des résiduels, etc. (*voir Boldina et Beninger 2016*)

Mar Biol (2007) 151:949–959
DOI 10.1007/s00227-006-0529-4

RESEARCH ARTICLE

Information-theory approach to allometric growth of marine organisms

Stelios Katsanevakis · Maria Thessalou-Legaki · Constantina Karlou-Riga · Eugenia Lefkaditou · Evagelos Dimitriou · George Verriopoulos

Received: 18 April 2006 / Accepted: 24 October 2006 / Published online: 22 November 2006

Abstract Allometric growth investigations are usually conducted by fitting the allometric model (L) $y = ax^b \Leftrightarrow \log y = \log a + b \log x$ (y, x are morphometric characters and b the allometric exponent), which is quite simple both conceptually and mathematically, and its parameters are easy to estimate by linear regression. However b is not necessarily constant and it may change either continuously or abruptly at specific breakpoints; thus, the simple L model quite often fails to describe allometric growth successfully. In the current context, a better alternative is proposed, based on Kullback–Leibler (K-L) information theory and multi-model inference (MMI). Allometric growth was investigated in eight marine species: the bivalves *Pecten jacobaeus* and *Pinna nobilis*, the squids *Todarodes sagittatus* and *Todaropsis eblanae*, the crab *Pachygrapsus marmoratus* (females), the ghost shrimp *Pestarella tyrrhena* (males), and the fishes *Trachurus trachurus* and *Sparus aurata*. In each of the eight species, a pair of body parts was measured and the allometric growth of one body part in relation to the other (reference dimension) was studied, by fitting five different candidate models including: the simple allometric model, two models assuming that b changed continuously and two other assuming that b had a breakpoint. For each species, the 'best' model was selected by minimizing the small-sample, bias-corrected form of the Akaike Information Criterion. To quantify the plausibility of each model, given the data and the set of five models, the 'Akaike weight' w_i of each model was calculated; based on w_i the average model was estimated for each case. MMI is beneficial, more robust, and may reveal more information than the classical approach. As demonstrated with the given examples, estimation of b from the linear model, when it was not supported by the data, revealed some characteristic pitfalls, such as concluding positive allometry when there is actually negative or vice versa, or reporting allometry when the data in reality support isometric growth or vice versa.

The information theory approach to model selection and inference is based on K-L information $I(f,g) = \int f(x) \log\left(\frac{f(x)}{g(x|\theta)}\right) dx$ (Kullback and Leibler 1951). $I(f,g)$ is the 'information' lost when model g (with parameters θ) is used to approximate full reality or truth f; equivalently $I(f,g)$ is interpreted as the distance from the approximating model to full reality (Burnham and Anderson 2002). According to information theory, minimization of K-L distance is a fundamental basis for model selection. Full reality f is unknown in real problems and thus $I(f,g)$ may not be computed directly. Akaike (1973) devised a method to approximate K-L distance, based on the empirical log-likelihood function. This is known as Akaike's information criterion (AIC) and is summarized by the formula $\mathrm{AIC} = -2\log(\mathcal{L}(\hat{\theta}|\mathrm{data})) + 2K$, where $\log(\mathcal{L}(\hat{\theta}|\mathrm{data}))$ is the numerical value of the log-likelihood at its maximum point, $\hat{\theta}$ is the vector of the estimated model parameters and K the number of estimable parameters.

Table 2 The candidate models used for allometric growth investigation

Name of model	Abbr.	k	Equation
Linear	L	3	$\log Y = a_1 + b_1 \log X$
Quadratic	Q	4	$\log Y = a_1 + b_1 \log X + b_2 (\log X)^2$
Cubic	C	5	$\log Y = a_1 + b_1 \log X + b_2 (\log X)^2 + b_3 (\log X)^3$
Broken-stick	BS	5	$\log Y = \begin{cases} a_1 + b_1 \log X, & X \le B \\ a_1 + (b_1 - b_2) \log B + b_2 \log X, & X > B \end{cases}$
Two-segment	TS	6	$\log Y = \begin{cases} a_1 + b_1 \log X, & X \le B \\ a_1 + b_2 \log X, & X > B \end{cases}$

Table 4 Values of AIC_c, AIC_c differences (Δ_i) and of the Akaike weights w_i for the five models of the measured morphometric variables, for each species. For each species, values corresponding to the best models are in *bold* characters

	P. jacobaeus	*P. nobilis*	*T. sagittatus*	*T. eblanae*	*P. marmoratus*	*P. tyrrhena*	*T. trachurus*	*S. aurata*
AIC_c								
L	**-1100.11**	-84.24	-82.43	-156.22	-64.31	-223.00	-314.79	-475.03
Q	-1099.53	-196.37	-92.25	-157.85	-64.21	**-228.47**	-320.95	-502.98
C	-1097.82	-195.14	-91.42	-155.68	**-83.12**	-227.20	-318.99	-507.59
BS	-1097.72	-204.81	-97.98	-158.76	-71.00	-227.70	-321.86	-515.26
TS	-1099.68	**-207.12**	**-102.48**	**-166.01**	-79.45	-227.75	**-330.95**	**-530.34**
Δ_i								
L	**0.00**	122.88	20.04	9.80	18.81	5.47	16.16	55.31
Q	0.58	10.74	10.23	8.16	18.91	**0.00**	10.01	27.36
C	2.29	11.98	11.06	10.34	**0.00**	1.27	11.96	22.75
BS	2.40	2.30	4.49	7.26	12.13	0.77	9.09	15.08
TS	0.43	**0.00**	**0.00**	**0.00**	3.67	0.72	**0.00**	**0.00**
w_i (%)								
L	**31.5**	0.0	0.0	0.7	0.0	2.2	0.0	0.0
Q	23.5	0.4	0.5	1.6	0.0	**33.7**	0.7	0.0
C	10.0	0.2	0.4	0.5	**86.0**	17.8	0.2	0.0
BS	9.5	23.9	9.5	2.5	0.2	22.9	1.0	0.1
TS	25.5	**75.6**	**89.6**	**94.6**	13.8	23.4	**98.0**	**99.9**

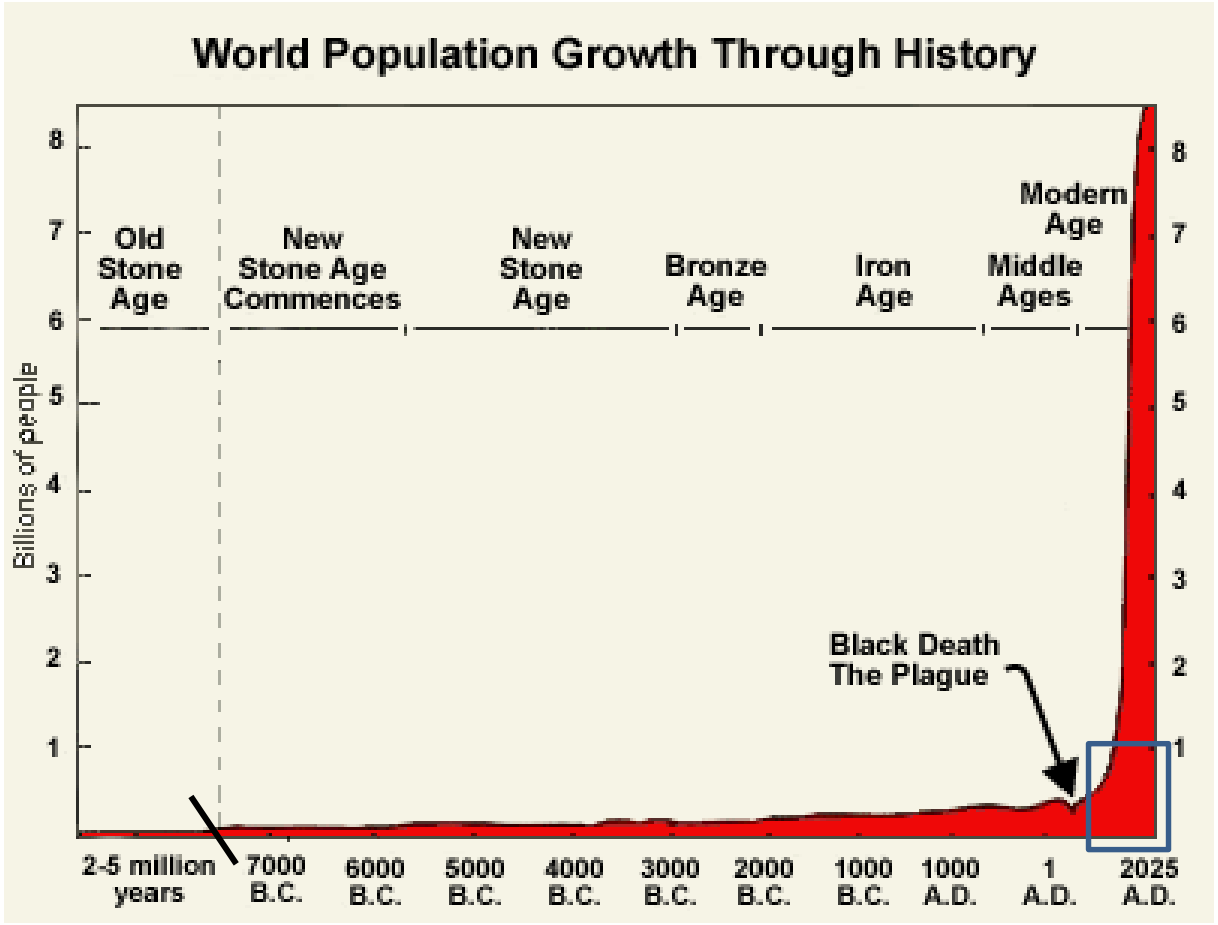
World Population Growth Through History
Billions of people
8
7
6
5
4
3
2
1
Old Stone Age
New Stone Age Commences
New Stone Age
Bronze Age
Iron Age
Middle Ages
Modern Age
Black Death
The Plague
2-5 million years
7000 B.C.
6000 B.C.
5000 B.C.
4000 B.C.
3000 B.C.
2000 B.C.
1000 B.C.
1000 A.D.
1 A.D.
2025 A.D.

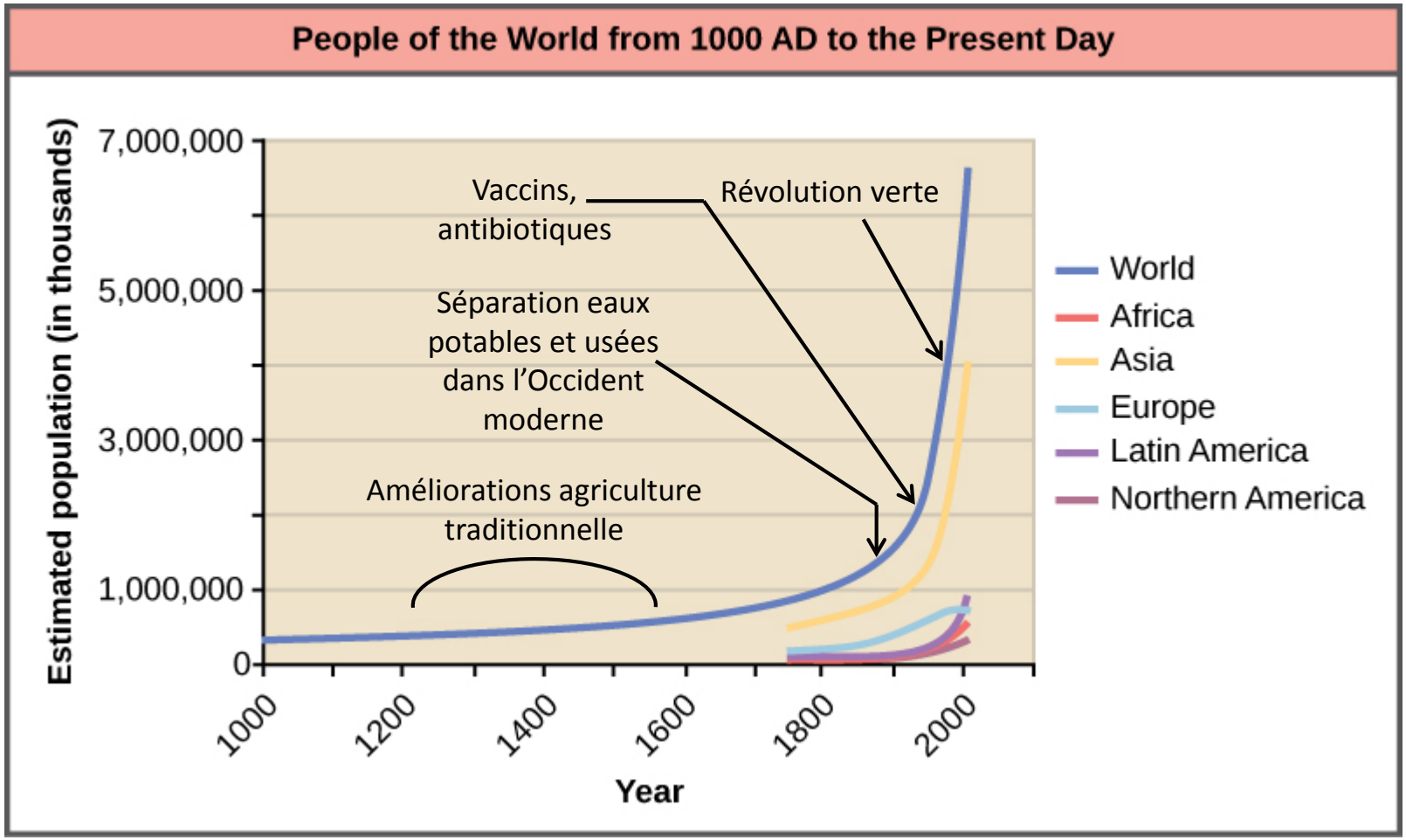
People of the World from 1000 AD to the Present Day
Estimated population (in thousands)
7,000,000
5,000,000
3,000,000
1,000,000
0
1000
1200
1400
1600
1800
2000
Year
Vaccins, antibiotiques
Révolution verte
Séparation eaux potables et usées dans l'Occident moderne
Améliorations agriculture traditionnelle
World
Africa
Asia
Europe
Latin America
Northern America

Exhibit 18: Demographic Transition Theory and its application to selected countries

Stages and current examples

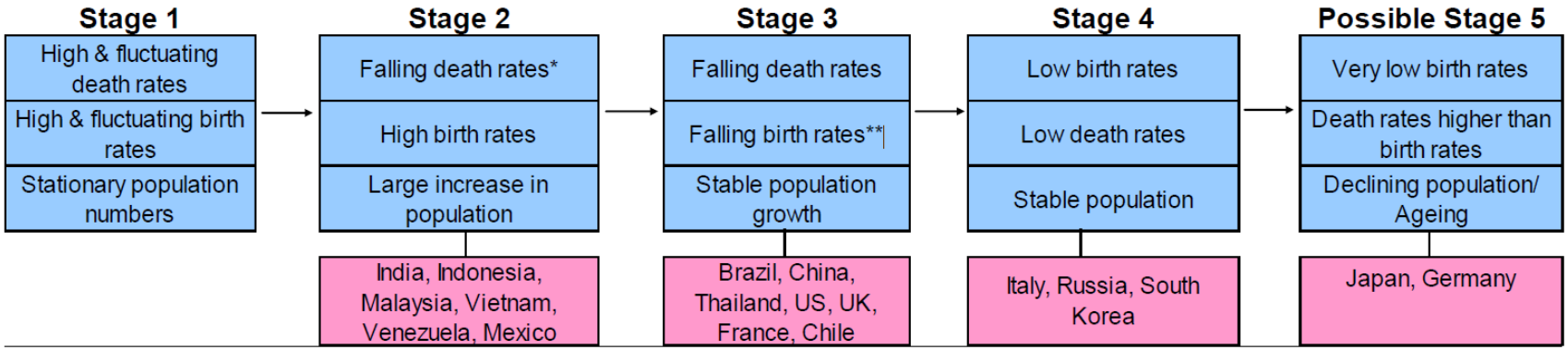

Source: Credit Suisse, *Demographic Transition Theory*, John Caldwell (2006)

*Reasons- Improvements in food supply, sanitation, technology, basic healthcare and education

**Reasons- Contraception, increases in wages, urbanization, reduction in subsistence agriculture, increase in the status and education of women, reduction in the value of children's work

La Mortalité

1. **Densité indépendante** ex: Désastre naturelle (incendie, éruption volcanique, inondation, sécheresse)

2. **Densité dépendante** ex: épidémie, prédation, chasse, compétition

Nous pouvons modeliser la mortalité densité-dépendante uniquement

Modelisation de la mortalité densité-dépendante

$dN/dt = -ZN$

Z = coefficient de mortalité instantanée totale (naturelle + capture)

En intégrant,

$N_t = N_0 e^{-zt}$

N_0 , t connus

Pour trouver Z, on prend les Log_e :

$Log_e N_t = Log_e N_0 – Zt$

Equation d'une droite, pente = Z

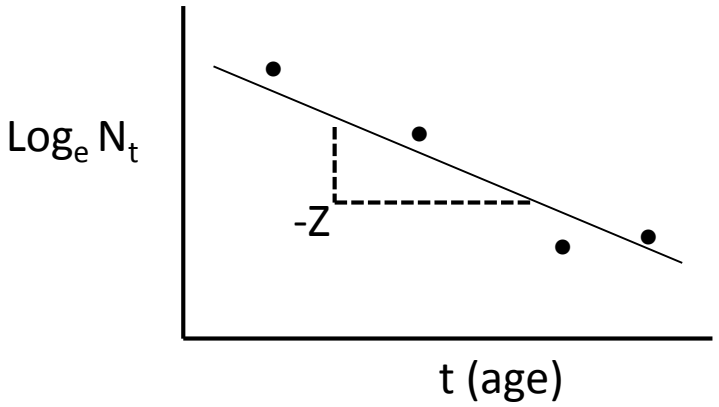

Cas de Z variable selon age

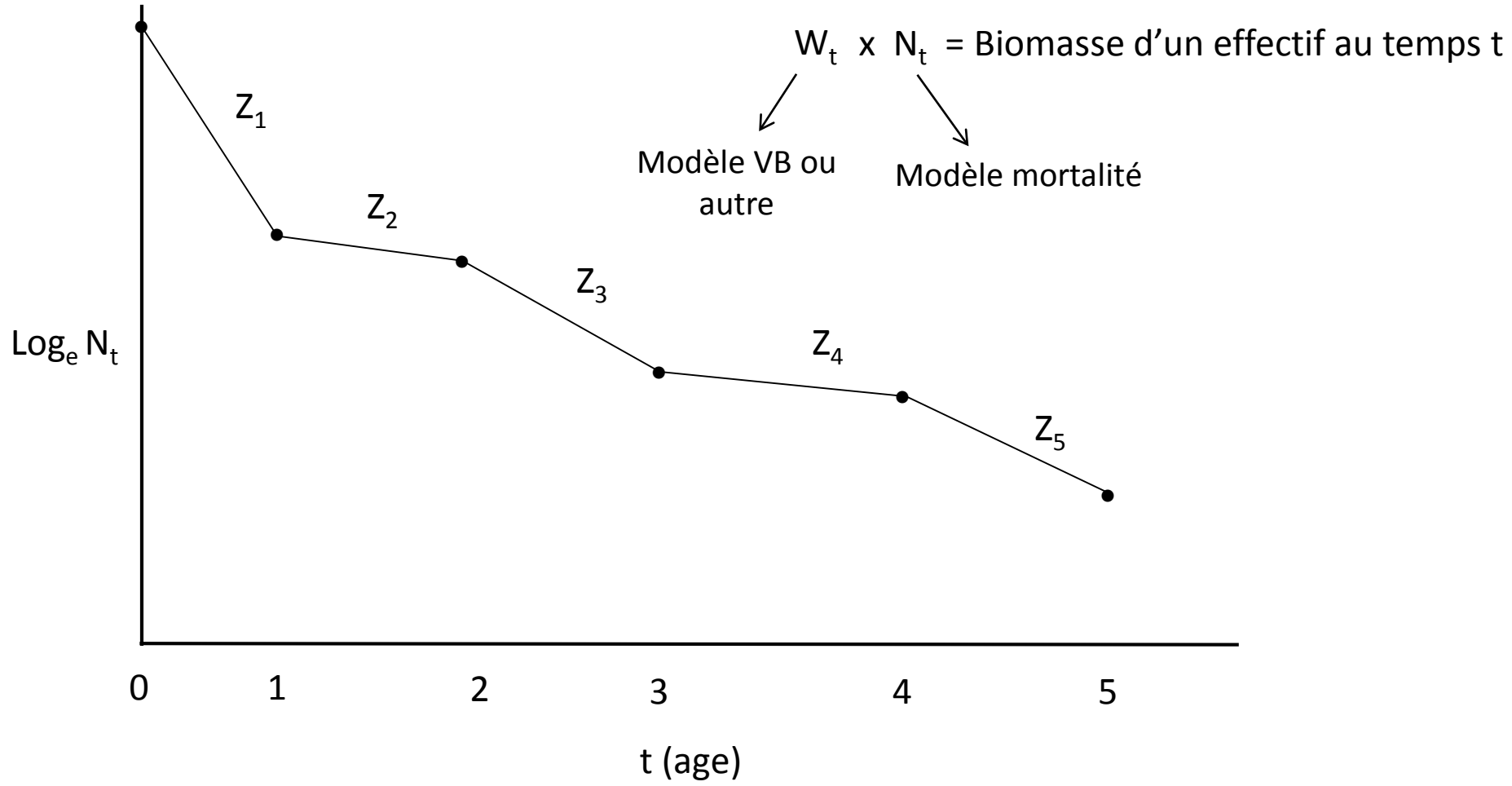

Séparation de la mortalité par capture (F, C) et la mortalité naturelle (M)

Etant connu la mortalité totale Z et l'effort de capture f,

$ZT = (F+M)T$, et comme $F = qf$, q = vulnérabilité, f= effort

$ZT = qf + MT$

Quand $T = 1$, ex: 1 mois, 1 année etc.

$Z = qf + M$ droite avec pente = q, int-y = M

Et comme $Z = M + F$,

$F = Z - M$

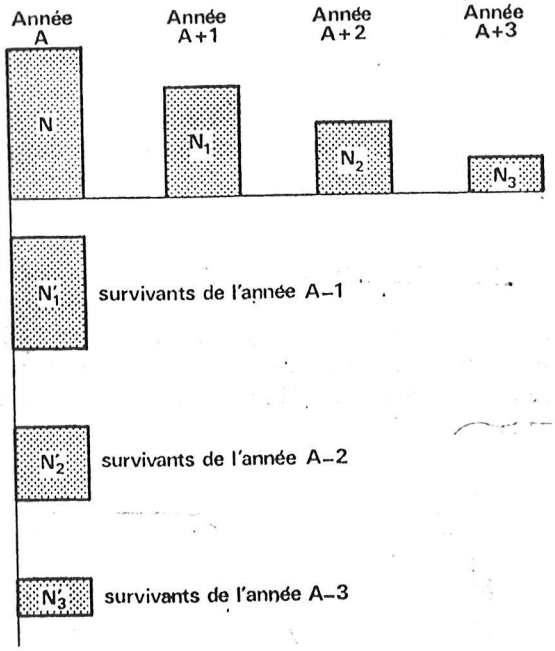

FIG. 2-3. — *Comparaison de la situation d'une pêcherie pour une année donnée* (année A) *et de l'évolution d'une classe d'âge au cours d'années successives* (de A à A + 3). Recrutement et mortalité sont supposés constants (voir texte).

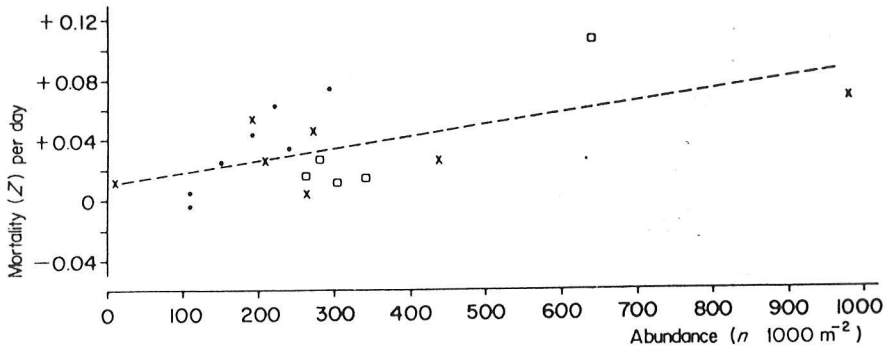

Figure 5.3 Density-dependent mortality of 0-group plaice at settlement in the Wadden Sea (van der Veer, 1986a); the samples were taken in 1980 (●), 1981 (X) and 1982 (□) (Reproduced by permission of Inter-Research)

Slow adaptation in the face of rapid warming leads to collapse of the Gulf of Maine cod fishery

Andrew J. Pershing,1* Michael A. Alexander,2 Christina M. Hernandez,1† Lisa A. Kerr,1 Arnault Le Bris,1 Katherine E. Mills,1 Janet A. Nye,3 Nicholas R. Record,4 Hillary A. Scannell,1,5‡ James D. Scott,2,6 Graham D. Sherwood,1 Andrew C. Thomas5

Several studies have documented fish populations changing in response to long-term warming. Over the last decade, sea surface temperatures in the Gulf of Maine increased faster than 99% of the global ocean. The warming, which was related to a northward shift in the Gulf Stream and to changes in the Atlantic Multidecadal and Pacific Decadal Oscillations, led to reduced recruitment and increased mortality in the region's Atlantic cod (*Gadus morhua*) stock. Failure to recognize the impact of warming on cod contributed to overfishing. Recovery of this fishery depends on sound management, but the size of the stock depends on future temperature conditions. The experience in the Gulf of Maine highlights the need to incorporate environmental factors into resource management.

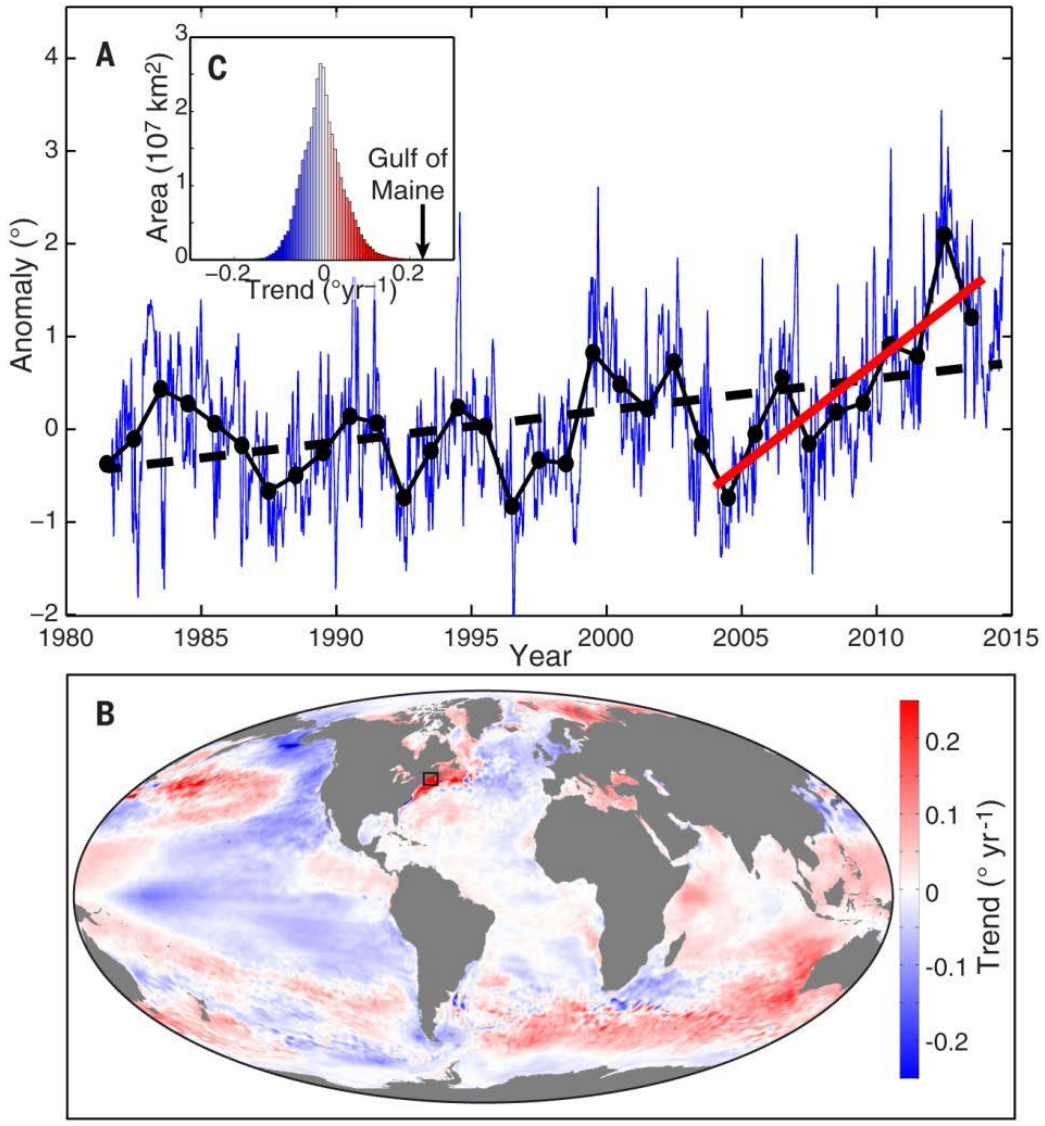

Fig. 1. Sea surface temperature trends from the Gulf of Maine and the global ocean. (A) Daily (blue, 15d smoothed) and annual (black dots) SST anomalies from 1982-2013 with the long-term trend (black dashed line) and trend over the last decade (2004-2013) (red solid line). (B) Global SST trends (° yr^{-1}) over the period 2004-2013. The Gulf of Maine is outlined in black. (C) Histogram of global 2004-2013 SST trends with the trend from the Gulf of Maine indicated at the right extreme of distribution.

29 October 2015 / Page 1 / 10.1126/science.aac9819

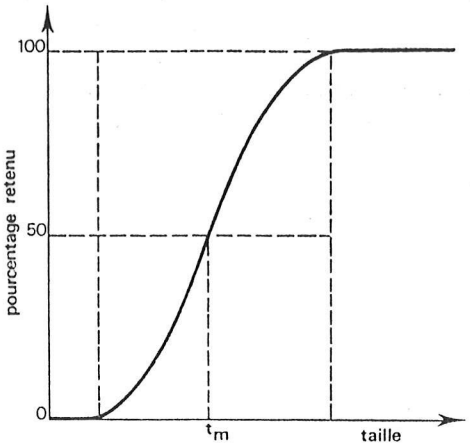

FIG. 2-6. — *Détermination du point 50 % sur la courbe de sélection.* Voir le texte pour la signification de t_m.

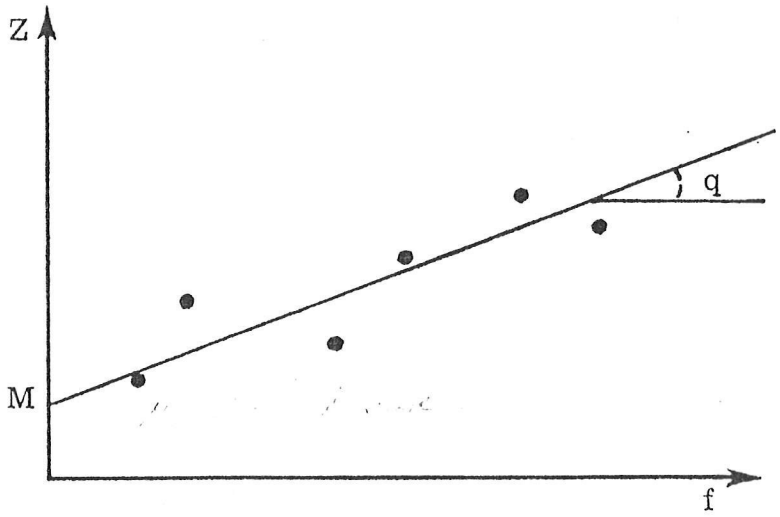

FIGURE 5.2. – Estimation de F et de M. Représentation graphique du coefficient de mortalité totale en fonction de l'effort de pêche

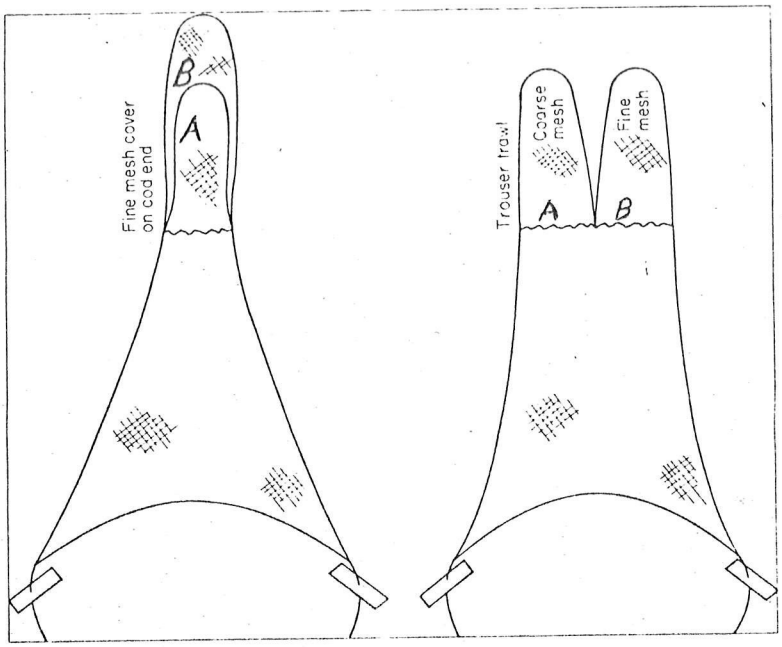

Fig. 6.13. Diagram of otter trawl nets rigged for mesh selectivity experiments. The mesh in the forward part guides the fish to the cod end where the filtering occurs.

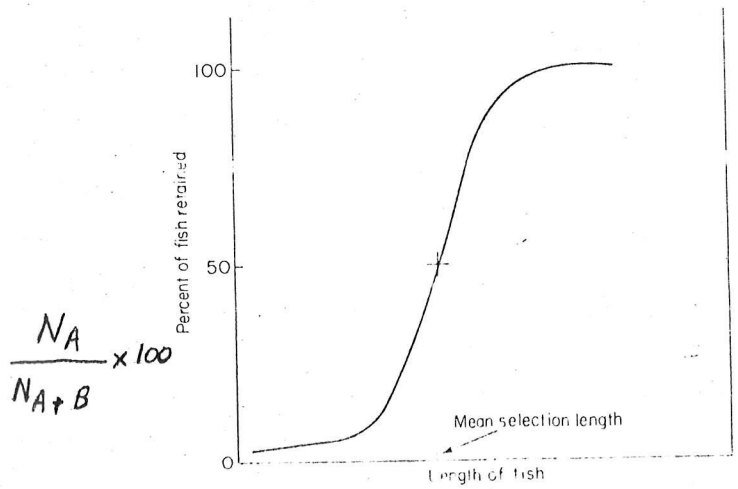

$$\frac{N_A}{N_{A+B}} \times 100$$

Fig. 6.14 Hypothetical selection curve for a trawl net. The lower end of the curve may not reach zero because some small fish become mixed with the bulk of the catch.

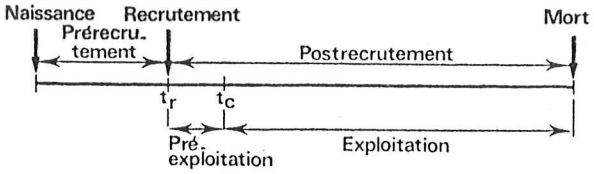

FIG. 2-2. — *Schématisation des différentes phases de la vie d'un poisson.* t_r : âge du recrutement; t_c : âge d'entrée dans les captures.

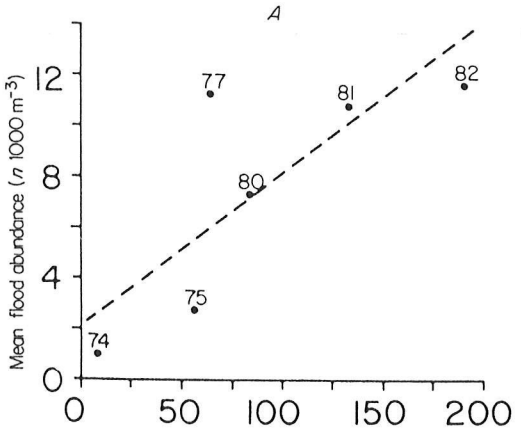

Figure 5.4 Dependence of an index of plaice recruitment on numbers of larval stage 4b in the flood waters of the Wadden Sea (van der Veer, 1986a) (Reproduced by permission of Inter-Research)

Fisheries Research, 4 (1986) 317–329
Elsevier Science Publishers B.V., Amsterdam — Printed in The Netherlands

The Utility of Artificial Collectors as a Technique to Study Benthic Settlement and Early Juvenile Growth of the Rock Crab, *Cancer irroratus*

PETER G. BENINGER, LORETTE CHIASSON and ROBERT W. ELNER[1]
Département de Biologie, Université de Moncton, Moncton, N.B. E1A 3E9 (Canada)

(Accepted for publication 30 June 1986)

ABSTRACT

Beninger, P.G., Chiasson, L. and Elner, R.W., 1986. The utility of artificial collectors as a technique to study benthic settlement and early juvenile growth of the rock crab, *Cancer irroratus*. *Fish. Res.*, 4: 317–329.

Concurrent studies of planktonic larval density and benthic recruitment of *Cancer irroratus* were performed in Kochibouguac Bay, New Brunswick, from late May to mid-September 1981. Three artificial collector types were used; mop, box and Witham. All collector types were shown to sample settling *C. irroratus*. Although *Homarus americanus* is also abundant in this region, no settling stages or young juveniles were observed in the collectors. The most efficient collector appears to be the mop type, which should be tethered off the bottom to avoid excessive clogging on mud bottoms.

The usefulness of these collectors in the study of growth of these otherwise inaccessible stages was demonstrated using modal analysis of size-frequency histograms. In addition, the presence of 26 exuviae (2.5–58 mm carapace width) showed that juveniles of all sizes molt in these collectors.

The larval density data revealed a clear sequence of events, comprising the appearance of the first zoea larvae in early summer, the presence of a large megalopa peak in mid-July, followed immediately by the appearance of new recruits ($\geq$ first crab stage) in the collectors. The use of such artificial collectors constitutes a promising technique in the study of benthic recruitment and early growth of *C. irroratus*.

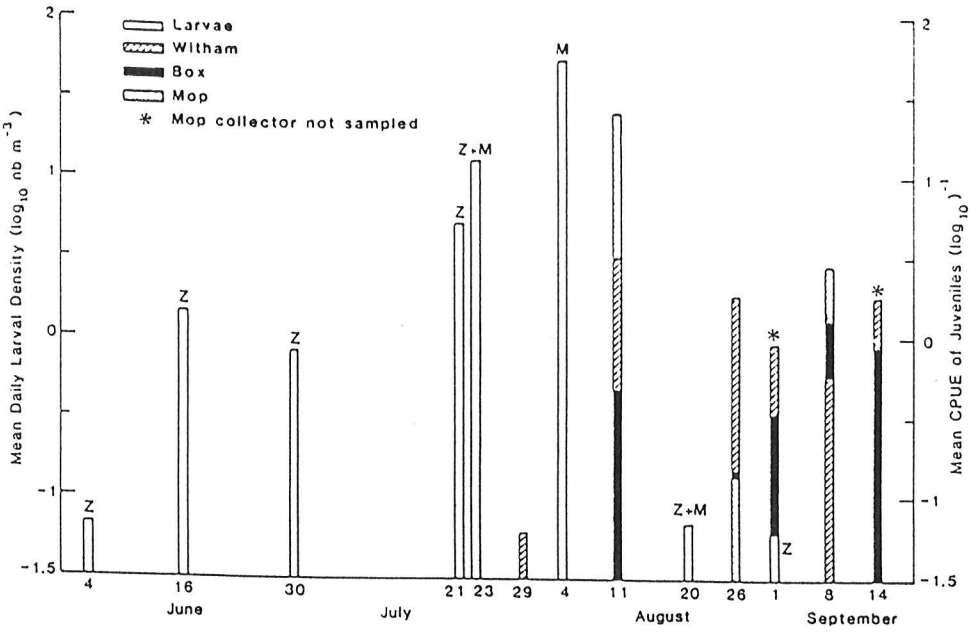

Fig. 3. Mean daily larval densities and mean CPUE of juveniles. Z = zoeal stage dominant (60% of all crab larvae); M = megalopa stage dominant.

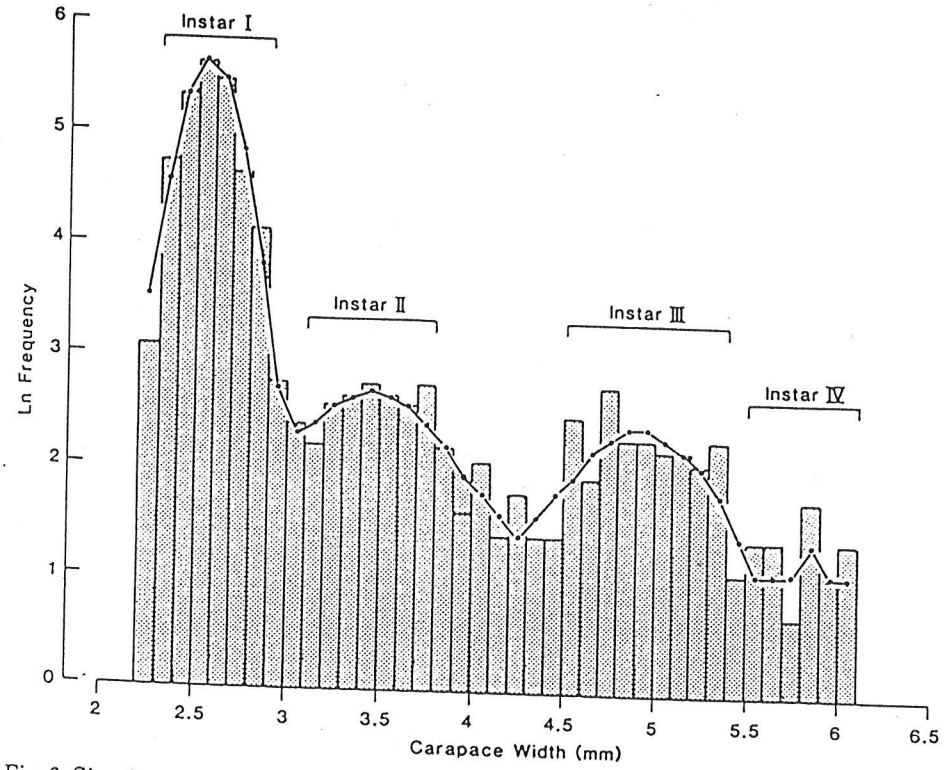

Fig. 6. Size-frequency histogram of all *C. irroratus* ⩽6 mm CW found in the collectors over the 4-month study period, with component normal distributions as calculated by the POLYMODE programme. Instar stages are indicated as deduced from data by Krouse (1976).

Fisheries Research, 6 (1987) 81–92
Elsevier Science Publishers B.V., Amsterdam — Printed in The Netherlands

Larval Settlement, Juvenile Growth and the Potential Use of Spatfall Indices to Predict Recruitment of the Scallop *Pecten alba* Tate in Port Phillip Bay, Victoria, Australia

B.L. SAUSE, D. GWYTHER and D. BURGESS

Marine Science Laboratories, Department of Conservation, Forests and Lands, P.O. Box 114, Queenscliff, Vic. 3225 (Australia)

(Accepted for publication December 19, 1986)

ABSTRACT

Sause, B.L., Gwyther, D. and Burgess, D., 1987. Larval settlement, juvenile growth and the potential use of spatfall indices to predict recruitment of the scallop *Pecten alba* Tate in Port Phillip Bay, Victoria, Australia. *Fish. Res.*, 6: 81–92.

Settlement of the scallop, *Pectan alba*, in artificial collectors and the growth of juvenile scallops were examined in relation to separately obtained estimates of annual recruitment in Port Phillip Bay, Southeastern Australia. A single, annual settlement during October–December was observed during the 3 year study. Settlement was greatest in collectors immersed for 2 months in the middle of the water column. Spat grew to 60 mm shell length during their first 12 months and attained a recruitment size of 70 mm within 16–18 months. Settlement during one year can, therefore, be related to recruitment during the next. From the data available so far, high and low settlement has been reflected in subsequent differences in recruitment. Though more years' data are required, indices of spatfall may provide managers of this industry with the possibility of predicting major fluctuations in recruitment 1 year in advance.

TABLE II

Comparison of spatfall indices with numbers of scallops recruited 1 year later

		Settlement index	Number of recruits 1 year later (millions of scallops)
1983/1984	East	700	108
	West	450	90
1984/1985	East	100	30
	West	100	18
1985/1986	East	600	
	West	200	

Contents lists available at ScienceDirect

Estuarine, Coastal and Shelf Science

journal homepage: www.elsevier.com/locate/ecss

Relationships between adult population size, recruitment, and year-class strength in a labrid fish in the Mediterranean Sea

Nuria Raventos

Centre d'Estudis Avançats de Blanes (CEAB-CSIC), Accés a la Cala San Francesc, n° 14. 17300 Blanes, Girona, Spain

ARTICLE INFO

Article history:
Received 10 March 2009
Accepted 19 July 2009
Available online 26 July 2009

Keywords:
parental stock
recruitment
stock-recruitment relationships
littoral fishes
NW Mediterranean Sea
Symphodus roissali

ABSTRACT

The influence of distinct demographic factors on determining population size in a littoral nesting fish (*Symphodus roissali*) was studied. Differences in the overall abundances were studied at three sites in the NW Mediterranean Sea for three years, to examine whether: 1) the adult population determined the number of successful nests; 2) the number of successful nests determined recruitment levels; 3) recruitment levels were subsequently related to the number of young of the year (YOY) joining the population after the recruitment period; and 4) the YOY value determined the size of the year class 1 cohort in the following year's adult reproductive population. The results show that there was a significant relationship between the number of spawners and the number of successful nests. However, the number of successful nests does not always correlate well with recruitment level. Furthermore, recruitment levels are not good indicators of the Young of the Year (measured three months after settlement) in number joining the populations, though YOY in number was related to the strength of the year class joining the adult reproductive population the following year. Therefore, the magnitude of the recruitment and probably the size of the adult population did not determine the year-class strength in *S. roissali*.

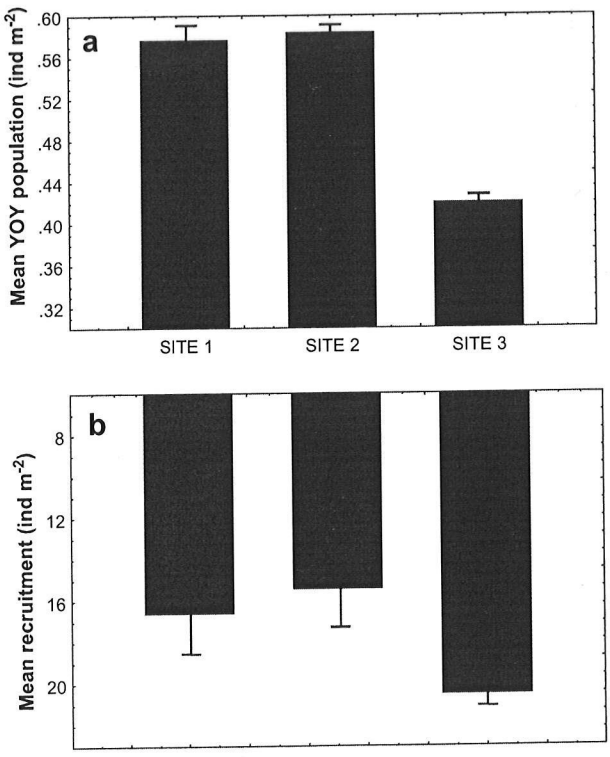

Fig. 3. a) Time series (1998–1999–2000) of mean population abundance at each sampling site; b) time series (1998–1999–2000) of mean recruitment at each sampling site.

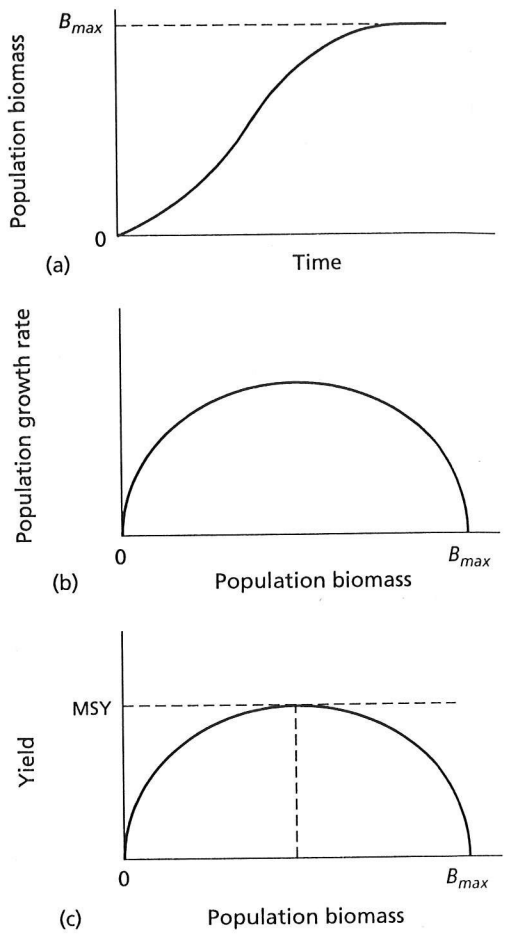

Fig. 7.3 (a) Logistic population growth. (b) Populations grow most quickly at intermediate sizes up to a maximum total biomass, B_{max}. (c) The maximum sustainable yield (MSY) in biomass occurs at a level of fishing mortality that places the population at an intermediate size.

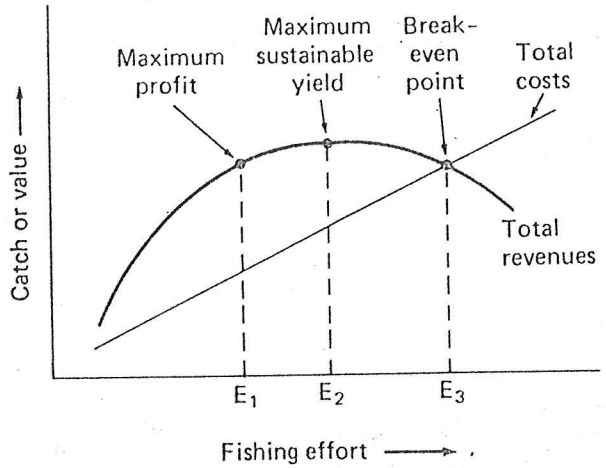

FIGURE 12-9 Fishing value as compared to fishing effort (number of boats, days at sea, and so forth). (From G. H. Knight, *International Law of Fisheries,* Louisiana State University Teaching Aid, Issue No. 2, Center for Wetlands Resources.)

Table 13.2 Global marine discards (includes bycatch landed but unreported by species in industrial fisheries) on the basis of the FAO International Standard Statistical Classification of Aquatic Animals and Plants species groups. From Alverson *et al.* (1994).

Species group	Mean discard weight (tonnes)	Landed weight (tonnes)	Ratio of discarded weight to landed weight	Ratio of discarded weight to total weight
Shrimps, prawns	9 511 973	1 827 568	5.20	0.84
Redfishes, basses, congers	3 631 057	5 739 743	0.63	0.39
Herrings, sardines, anchovies	2 789 201	23 792 608	0.12	0.10
Crabs	2 777 848	1 117 061	2.49	0.71
Jacks, mullets, sauries	2 607 748	9 349 055	0.28	0.22
Cods, hakes, haddocks	2 539 068	12 808 658	0.20	0.17
Miscellaneous marine fishes	992 356	9 923 560	0.10	0.09
Flounders, halibuts, soles	946 436	1 257 858	0.75	0.43
Tunas, bonitos, billfishes	739 580	4 177 653	0.18	0.15
Squids, cuttlefishes, octopuses	191 801	2 073 523	0.09	0.08
Lobsters, spiny-rock lobsters	113 216	205 851	0.55	0.35
Mackerels, snooks, cutlassfishes	102 377	3 722 818	0.03	0.03
Salmons, trouts, smelt	38 323	766 462	0.05	0.05
Shads	22 755	227 549	0.10	0.09
Eels	3 359	9 975	0.84	0.46
Total	27 012 099	76 999 942	0.35	0.26

Table 13.3 The 20 fisheries with the highest recorded discard ratios by weight (discarded weight per landed target catch weight) and the 10 fisheries with the lowest observed weight-based discard ratios. After Alverson *et al.* (1994).

Fishery description	Kg discarded per kg landed
Highest discard ratios	
Trinidadian shrimp trawl	14.71
Indonesian shrimp trawl	12.01
Australian northern prawn trawl	11.10
Sri Lankan shrimp trawl	10.96
US Gulf of Mexico shrimp trawl	10.30
Sea of Cortes shrimp trawl	9.70
Brazilian shrimp trawl	9.30
West Indian shrimp trawl	8.52
US Southeast shrimp trawl	8.00
Northwest Atlantic fish trawl	5.28
Persian Gulf shrimp trawl	4.17
Southwest Atlantic shrimp trawl	4.10
East Indian shrimp trawl	3.79
Bering Sea sablefish pot	3.51
Malaysian shrimp trawl	3.03
Senegalese shrimp trawl	2.72
Bering Sea rock sole trawl	2.61
British Columbia cod trawl	2.21
Gulf of Alaska flatfish trawl	2.08
Northeast Atlantic dab trawl	2.01
Lowest discard ratios	
Northwest Atlantic hake trawl	0.011
West Central Atlantic menhaden seine	0.029
Bering Sea cod pot	0.041
Northeast Pacific whiting trawl	0.043
Northwest Atlantic cod trawl	0.058
Bering Sea Pelagic pollock trawl*	0.062
Northwest Atlantic redfish trawl	0.063
Northeast Atlantic groundfish trawl	0.083
Gulf of Alaska midwater pollock trawl	0.086
Northwest Atlantic plaice trawl	0.118

* Includes some on-bottom fishing.

Le processus décisionnel de la gestion d'un stock